Citation Info:
Deiler, Christoph and Fezans, Nicolas (2020) Performance-Based Ice Detection Methodology, Journal of Aircraft 57:2, 209-223. doi: 10.2514/1.C034828

Performance-Based Ice Detection Methodology

Christoph Deiler*, Nicolas Fezans†

DLR (German Aerospace Center), Braunschweig, 38108, Germany

A novel robust ice detection methodology for the early detection of icing related flight performance degradation is presented. Based on data of 75,689 flights with modern commercial airliners, a maximum aircraft fleet's performance variation has been estimated. The evaluation of results indicates that an expected influence of icing could be clearly separated. The developed methodology is energy-based and fuses aircraft body and engine influences on flight performance, which allows to reliably calculate a deviation from an available reference. This difference in flight performance is consequently used to detect an aerodynamic degradation. The novel methodology provides large capabilities and shows a good detection reliability with no false alarm even within maneuvering flight, wind shear, turbulence and sideslip as well as for several sensor error cases. The methodology was evaluated during various simulator trials. The results show a very high potential in supporting pilots with adequate information about the current aircraft status in icing conditions.

Nomenclature

α	angle of attack, rad
β	angle of side slip, rad
$\delta_{\text{Detection}}$	detection flag
Δf	function
δl	distance, m

*Research Scientist, Institute of Flight Systems, Lilienthalplatz 7, Braunschweig, 38108, Germany
†Research Scientist, Institute of Flight Systems, Lilienthalplatz 7, Braunschweig, 38108, Germany

η	elevator deflection, rad
Φ	bank angle, rad
ξ	aileron deflection, rad
ζ	rudder deflection, rad
k_2	drag coefficient factor
$C_{(\cdot)}$	aerodynamic coefficient
C_{L0}	lift coefficient at $\alpha = 0$
C_D	drag coefficient
C_{D0}	zero-lift drag coefficient
$(\Delta C_D)_{\text{crit}}$	drag coefficient threshold
$\Delta C_{\widetilde{D}}$	equivalent drag coefficient
C_L	lift coefficient
C_{lp}	roll damping coefficient
C_{nr}	yaw damping coefficient
c_1, $\alpha^\star$	separation point function parameter
D	drag force, N
e	Oswald factor
$\dot{E}$	energy change resp. power, W
g	gravitational acceleration, m/s^2
H	altitude, m
$k_{(\cdot)}$	icing model factor
k_{ice}	icing severity factor
k_2	parameter influencing the drag polar curvature
L	lift force, N
Λ	wing aspect ratio
Ma	Mach number
m_{AC}	aircraft mass, kg
$\dot{m}_{\text{Fuel}}$	fuel flow, kg/s
n	load factor
N_1	engine fan speed, %

$\mathcal{O}(\cdot)$	order of magnitude
P	model parameter
$\mathcal{P}$	percentile/ quantile
$\overline{q}$	dynamic pressure, Pa
S_{Wing}	wing surface area, m^2
t	time, s
T_{stat}	static air temperature, K
u, v, w	translational velocities, m/s
V	velocity, m/s
$\widehat{X}$	non-dimensional wing separation point
x, y, z	body fixed coordinates, m
a	aerodynamic reference frame
ATRA	advanced technology research aircraft
AVES	air vehicle simulator
base	base model part
CAS	calibrated airspeed
comp	compensation term
corr	corrected
ECAM	electronic centralized aircraft monitor
FAR	federal aviation regulation
FDR	flight data recorder
IAS	indicated airspeed
ice	Δ-model part (icing)
IPS	ice protection system
k	kinetic reference frame
MCI	model confidence index
opt	optimal
QAR	quick access recorder
ref	reference
SLD	supercooled large droplets

TAS	true airspeed
tot	total
w	wind induced
WB	wing/body

I. Introduction

Icing can have a hazardous impact on the aircraft performance. In case of icing aircraft operational limitations might need to be adapted to remain in a safe flight envelope. During the last decades various accidents worldwide have shown the potential severity of icing-induced degradations as well as pilot's difficulties to recognize and cope with the corresponding changes in aircraft behavior [1–3].

The main degradation due to airframe (especially wing) icing manifests itself in a reduced stall angle of attack and increased drag. In the past, these effects of the icing phenomena have been investigated in various studies for different airfoils and icing cases (e.g. Refs. [4–6]) as well as for complete aircraft [7–10]. Figure 1 illustrates the typical estimated icing-induced modification of the lift and drag curves as generally described e.g. in the AGARD report 344 [4]. One major effect of aircraft ice accretion is a significant drag increase due to surface roughness changes, parasitic influence of ice protuberances, and local flow separation. Another effect of icing is a change of the aircraft lift behavior, with nonlinearities in the lift curve starting at a lower angle of attack than on the clean profile/wing (e.g. earlier or more abrupt flow detachment with increasing angle of attack).

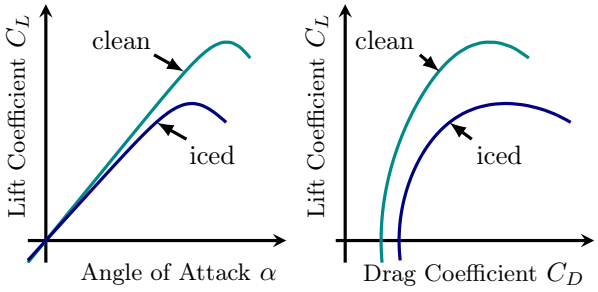

Figure 1. Expected aerodynamic degradation due to icing [4] (lift curve and drag polar)

Modern aircraft are equipped with anti-ice systems preventing ice accretion on critical parts or de-icing installations to remove ice shapes with a certain size. But these systems mainly are designed to fulfill existing certification requirements (e.g. FAR part 25

Appendix C [11]), which do not cover all icing types like e.g. supercooled large droplets (SLD) icing (nowadays covered by Appendix O to e.g FAR part 25 [11]). This means, that for existing aircraft there is a remaining (yet relatively remote) risk of ice accretion. Furthermore, all different existing ice protection systems (IPS) require an additional significant amount of energy on board. In case of thermal protection systems usually bleed air is used, which causes a reduction of the engine effectiveness and an increased fuel consumption. A deliberate activation of the IPS is necessary for efficient flight operations, which raises the demand for a reliable information about the current degradation, safety risk, and therefore need to activate the IPS. This information could be provided by the herein proposed detection method.

This paper presents a novel methodology and system for the on-board surveillance of aircraft performance and its use for ice detection purposes. By providing pilots with a warning at a very early stage of ice accretion, aircraft safety is significantly increased in icing conditions, which was already shown by Bragg et al. in Ref. [12]. At that very stage, anti-ice/de-ice can be applied as countermeasures and the region in which icing conditions are encountered could still be left safely. The system with the herein proposed detection methodology can provide crucial information to the pilots while only requiring the sensor information that is available on all modern airliners and business jets. The developed system relies on the change in flight performance (i.e. steady flight states) contrary to the many failed attempts (e.g. in Refs. [12–17]) based on the estimation of changes in the aircraft's dynamic behavior. The change/degradation in the flight performance is an indicator of ice accretion that is both robust and highly available: unlike the approaches based on the detection of changes in the aircraft dynamical behavior, it can be used also during steady flight conditions (most of an operating flight) and can detect icing effects significantly before approaching stall. Apart from the safety improvements provided by this detection method, a more targeted use of extremely energy-consuming devices such as anti-ice systems could possibly be enabled. Nevertheless, other approaches for detection of icing conditions, for example using already existing sensor technologies on e.g. measuring ice accretion on a probe [18] or a the thermal dissipation on a probe in free stream [19], or ice accretion on the airframe, for example using ultrasonic guided

waves [20, 21], could deliver a partly similar information, but rely on additional sensor technology and/or would require (a potentially costly) modification of existing and future aircraft.

In section II of this paper, the major effects of icing on aircraft are described. Furthermore, a necessary extension of the aerodynamic model to represent these effects in the simulation is given. Section III presents a first feasibility study that was made based on data recorded by the German airline TUIfly during their regular operations. A brief descriptions of detection methodology and system implementation are given in section IV. First results to proof the detection reliability on the example of the DLR Airbus A 320 "ATRA" (*Advanced Technology Research Aircraft*) are finally shown in section V.

II. Icing Effects on Aircraft

The degrading effects of icing on aerodynamics are still a concern for modern aircraft. Although most commercial aircraft are equipped with suitable countermeasures, fatal accidents happened over the years because the IPS was not activated or failed in terms of removing ice accretion of critical parts. Furthermore, current systems could not successfully prevent ice accretion for every icing condition, for what reason the certification rules had been adapted (Appendix O for SLD icing [11, 22, 23]).

An aircraft's aerodynamics are strongly influenced by ice accumulation on or near the lifting surface leading edges. As shown in Fig. 1, the aerodynamic performance and therefore aircraft flight performance is generally degraded. This major effect is also well detectable in data records from e.g. flight test with natural or artificial ice shapes, whereas changes in the dynamic behavior are more difficult to detect reliably. Several attempts to model the icing influence on aircraft behavior had been conducted in the past with notable success. Based on the knowledge published on these modeling approaches [24–27] a novel way to model aircraft icing effects including a validation of the developed model formulation with flight test data was given in Ref. [28] and demonstrated using real flight data of a light business jet for two different artificial ice shapes [28]. The model formulation used was able to represent well the effects of icing on the test aircraft. A

comparison of the simulated lift and drag force coefficients and the coefficients calculated from measurements is given in Fig. 2 for the run-back ice case of Ref. [28]. The significant drag increase due to ice accretion is visible on the right plot in Fig. 2, whereas there is only a minor influence on the aircraft's lift behavior in the left plot. Similar results [28] are given in Fig. 3 for a leading edge icing case, but in contrast to Fig. 2 with a presumable flow separation for medium angles of attack. Based on the information about the aerodynamic degradation in Ref. [28] and the results in Refs. [12, 24–27] and Ref. [4] a generic icing model with a simple model structure comparable to the one presented in Ref. [29] was developed. For the evaluation of the new ice detection methodology, this generic icing model was added to the dynamic simulation model of DLR's research aircraft "ATRA" (Airbus A 320) as presented hereafter.

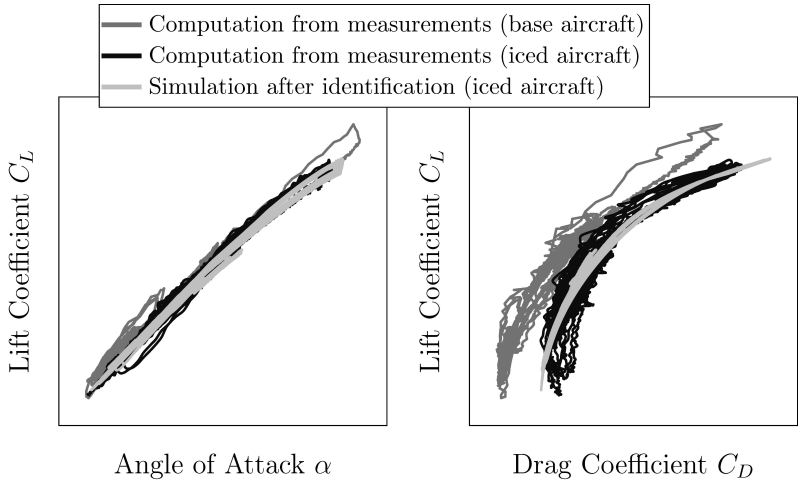

Figure 2. Lift curve and drag polar comparison between measured and simulated data for the artificial run-back ice accretion case (Ref. [28])

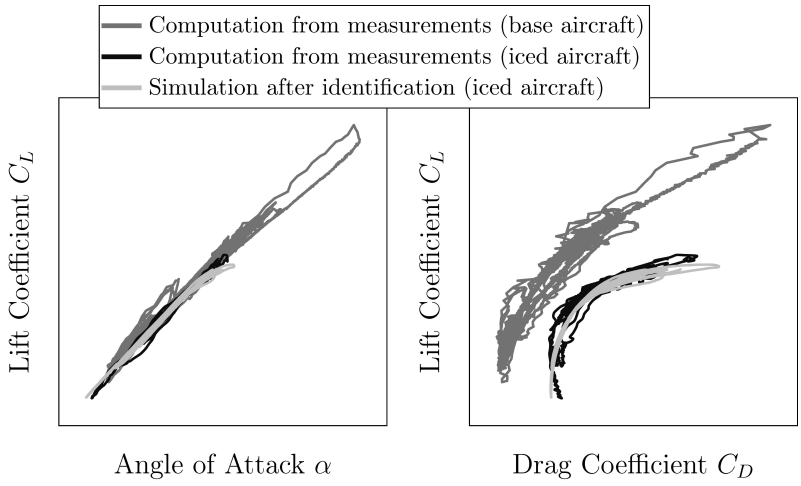

Figure 3. Lift curve and drag polar comparison between measured and simulated data for the artificial leading edge ice accretion case (Ref. [28])

II.A. Clean Aircraft Aerodynamics

The clean aircraft aerodynamic model – without icing – is formulated as a state of the art derivative model [30]. A specificity of this model is that the longitudinal aerodynamics are expressed as a two-point model [31], splitting wing and horizontal tailplane influences. In addition to the modeling of the "standard" aerodynamic effects, a nonlinear, unsteady wing lift curve is considered, which allows to simulate flow separation and reattachment effects [32]. The associated drag variation (i.e. with the flow separation) is also modeled. Both effects are modeled using the non-dimensional steady wing flow separation point position $\widehat{X}$

$$\widehat{X} = \frac{1}{2} \cdot \big(1 - \tanh\left(c_1 \cdot (\alpha - \alpha^\star)\right)\big), \tag{1}$$

as proposed in Ref. [33] and where $\alpha^\star$ denotes the angle of attack for which the wing flow is half separated (at 50% of the chord). The simplified wing/body lift coefficient equation including stall – considering Kirchhoff's theory of flow separation from the trailing edge – results in

$$C_{L,\mathrm{WB}} = C_{L0} + C_{L\alpha,\mathrm{WB}} \cdot \left(\frac{1 + \sqrt{\widehat{X}}}{2}\right)^2 \alpha. \tag{2}$$

The basic drag equation comprises the three main effects: zero lift drag, lift-induced drag and stall-related additional drag. It is expressed as follows

$$C_D = C_{D0} + \frac{1}{e\pi\Lambda} C_{L+}^2 \frac{\partial C_D}{\partial \widehat{X}} \left(1 - \widehat{X}\right). \tag{3}$$

Note that the base aircraft model formulation used here is similar to the ones presented in Refs. [28, 34], where comparable approaches to account for icing effects were proposed.

II.B. Iced Aircraft Aerodynamics

The basic idea is to use linearly altered parameters for icing-induced aerodynamic changes in aircraft simulation, which was introduced by Bragg et. al. [35]. Hence, a model parameter P is assumed to consist of a basic model part P_{base} and an additional Δ-model

part ΔP_{ice} describing the icing-induced changes:

$$P = (1 + k_P) \cdot P_{\text{base}} = P_{\text{base}} + \Delta P_{\text{ice}} \tag{4}$$

The additional factor k_P is used to model the degraded aircraft aerodynamics. As a result, all aerodynamic model coefficients which depend on an extended parameter P can be expressed as

$$C_{(\cdot)}(P) = C_{(\cdot)}\left(P_{\text{base}} + \Delta P_{\text{ice}}\right) = \big(C_{(\cdot)}\left(P_{\text{base}}\right)\big)_{\text{base}} + \Delta\big(C_{(\cdot)}\left(P_{\text{base}} + \Delta P_{\text{ice}}\right)\big)_{\text{ice}}, \tag{5}$$

where $C_{(\cdot)}$ represents the considered coefficient. Hence, the non-dimensional steady wing flow separation point in Eq. (1) is given by

$$\widehat{X}_{\text{base}} + \Delta\widehat{X}_{\text{ice}} = \frac{1}{2} \cdot \left(1 - \tanh\big(\,(1 + k_{c_1}) \cdot c_1 \cdot (\alpha - (1 + k_{\alpha^\star}) \cdot \alpha^\star)\,\big)\right). \tag{6}$$

This extension of the separation point formulation permits to account for a change in the stalling behavior of the iced aircraft. The icing effects can be introduced in the simplified lift coefficient of Eq. (2) as follows:

$$\begin{aligned} C_{L,\text{WB}_{\text{base}}} + \Delta C_{L,\text{WB}_{\text{ice}}} = {} & (1 + k_{C_{L0}}) \cdot C_{L0} \\ & + \left(1 + k_{C_{L\alpha,\text{WB}}}\right) \cdot C_{L\alpha,\text{WB}} \cdot \left(\frac{1 + \sqrt{\widehat{X}_{\text{base}} + \Delta\widehat{X}_{\text{ice}}}}{2}\right)^2 \alpha \end{aligned} \tag{7}$$

This also models a change in lift slope and a lift change at $\alpha = 0\,^\circ$ due to $k_{C_{L\alpha,\text{WB}}}$ and $k_{C_{L0}}$. The change $\Delta C_{D\text{ice}}$ in the drag coefficient mainly consists of an increased zero lift drag and modification of the lift-induced drag. Therefore the formulation given in Eq. (3) is extended to account for these effects:

$$C_{D\text{base}} + \Delta C_{D\text{ice}} = (1 + k_{C_{D0}}) \cdot C_{D0} + \frac{(1 + k_{k_2})}{e\pi\Lambda}\left(C_{L,\text{WB}_{\text{base}}} + \Delta C_{L,\text{WB}_{\text{ice}}}\right)^2, \tag{8}$$

where $k_{C_{D0}}$ represents the icing-induced change of zero lift drag, whereas k_{k_2} parametrizes the change of drag polar curvature.[‡]

The generic icing curves shown in Fig. 4 for DLR's Airbus A 320 are based on a light to moderate generic degradation with an increased zero lift drag, a higher polar curvature and a reduced stall angle of attack as defined by the parameters given in table 1.

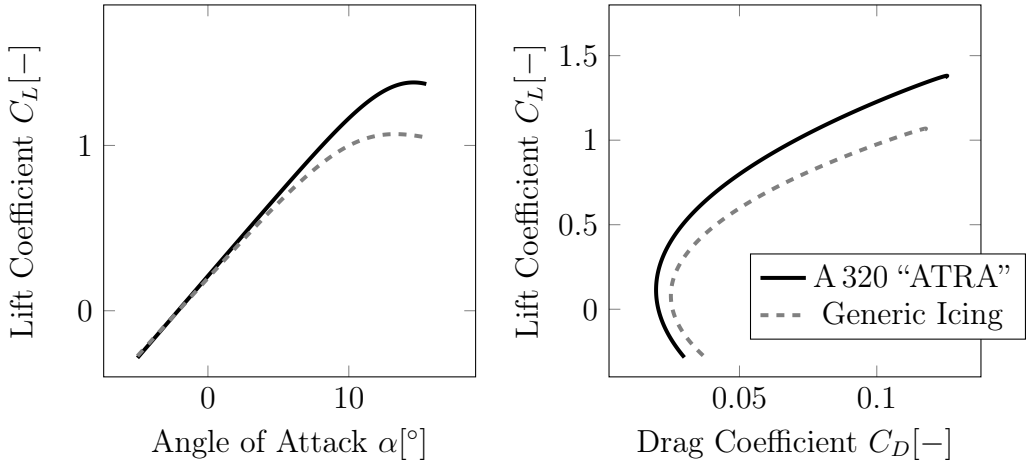

Figure 4. Comparison of Airbus A 320 "ATRA" lift and drag curve with and without generic icing influence

Table 1. Generic icing model parameters

flow separation	k_{c_1}	−0.20
	$k_{\alpha^\star}$	−0.20
lift coefficient at $\alpha = 0\,°$	$k_{C_{L0}}$	−0.05
lift slope (wing/body)	$k_{C_{L\alpha,\mathrm{WB}}}$	−0.05
zero lift drag coefficient	$k_{C_{D0}}$	0.25
drag polar curvature	k_{k_2}	0.50

III. Nominal Variation of Flight Performance within a Fleet

III.A. Challenges in Flight Performance Determination

There has been several noticeable previous works related to the extraction of flight performance from flight data recorder datasets, e.g. Ref. [36], or to estimate in real-time, aboard the aircraft, the impact of an icing-induced aerodynamics deterioration on the flight safety and on the safe flight envelope [37]. However, these approaches are not well suited for the considered case. For instance, the proper estimation of dynamic derivatives

[‡]the curvature of the drag polar can be represented by Oswald factor e and aspect ratio Λ, which is similar to the Taylor series factor $k_2 = (e\pi\Lambda)^{-1}$

(C_{lp}, C_{nr}, etc.) requires some amount of excitation of the aircraft, which is usually not present in data recorded on-board with the flight data recorder (FDR) and even if some relatively aggressive maneuvers would have been flown, the sampling rate of FDR data is usually too low to permits this kind of modeling. Note that even for on-board real-time performance monitoring (for which the sampling rate is sufficient), the need for dynamic excitation is a strong disadvantage for the application to civil airliners in regular operations. Fortunately, the performance monitoring technique presented in this paper does not require dynamic excitations but relies on the information already contained in the achieved steady state conditions. The goal and the approach of Ref. [36] is very similar to the FDR data analysis shown in this section, but the analysis that is presented here focuses more on pure performance (no dynamic derivatives) and is more general e.g. 1g flight is not assumed here whereas it is implicitly assumed in Ref. [36].

III.B. Performance Variation based on Aircraft Power Imbalance

Within a fleet of a single aircraft type the flight performance characteristics of each individual aircraft slightly differs. Some of the factors causing the flight performance variations across airplanes from the same type are:

- production tolerances,
- aircraft skin repairs,
- aircraft skin contamination (e.g. dirt),
- engine aging causing reduced efficiency,
- or engine contamination (e.g. dirt).

In order to be able to detect icing through the detection of flight performance changes, the other factors (i.e. nonrelated to icing) must be significantly lower than the degradations caused by icing. The methodology proposed hereafter (section IV) uses the standard aircraft sensors and the measurement error (calibration and noise) also introduces variations in the determination of the aircraft flight performance.

All in all, the aircraft flight performance can be seen as follows

$$\begin{aligned}\textbf{Flight Performance} = &\text{ Nominal Aircraft Flight Performance}\\ &+ \text{ Nominal Engine Influence}\\ &+ \textit{ Variation}\end{aligned}$$

whereby the "*Variation*" part gathers the effects mentioned previously and is here the part that need to be analyzed.

In order to determine the typical and most extreme flight performance variation encountered during regular airline operations (due to a real performance variation or sensor errors), data of 75,689 flights with Boeing B 737-700 and B 737-800 aircraft operated by TUIfly are analyzed. For the sake of this analysis, it is assumed that the major and statistically relevant noticeable flight performance variation in this data set result from the effects mentioned above. The data set contains regular flights with no particular incident. Whilst there is no absolute guarantee that this data set does not include flights in severe icing conditions or other abnormal conditions, it is certain that only a very restricted number of data points could be affected such that their influence on the herein described processing can definitely be neglected. The data of each flight was recorded with the quick access recorder (QAR), which receives the same signals as the flight data recorder, and downloaded by the airline after the flight. The data time resolution of the individual signals ranges from 8 Hz (e.g. accelerations) to 1/64 Hz (e.g. gross weight). No direct information about the aircraft thrust was recorded in the data and no engine simulation model permitting the calculation of these values out of measured engine parameters was available. This posed some difficulties for the intended analysis due to the major role played by the engines in the aircraft performance. This problem could be overcome acceptably well thanks to the huge quantity of data available. This was done by a segmentation in relatively short time-slices of about 60 s duration during which the aircraft was flying in a quasi-steady state: stabilized flight path (possibly climbing or descending) and possibly turning. Data segments with very dynamical maneuvers (e.g. high roll rate or rapid variation of load factor) were ignored in this analysis. Later on the segments are categorized according to their average speed, altitude, fan speed and outside air tem-

perature. Each category describes an engine operating point allowing the estimation of a linear model describing the engine influence on the flight performance.

Unfortunately the data used for this analysis were partly anonymized such that the correspondence between a particular airplane and a recorded flight data was not available. As a consequence, all available information of the fleet is used together to estimate a global engine influence for the B 737-700 and the B 737-800 separately. Note that for this analysis it is crucial to consider the data from all the aircraft of the same type since the aim is to compensate the missing engine data/information but not to adjust the performance for each individual aircraft. The unavailability of the correspondence information prevented the detection of outliers in the data, which for instance happen if one of the airplanes has a significantly better or worse performance than the others. Eventually, this process enabled to obtain an acceptable estimate of the missing information on the engines, but a real engine model would probably have been significantly more precise.

The methodology used to derive the aircraft performance from the recorded data is based on the energy of the airplane or rather its time-derivative. The total energy of the aircraft is

$$E_{\text{tot}} = \frac{1}{2} \cdot m_{\text{AC}} \cdot V_{\text{TAS}}^2 + m_{\text{AC}} \cdot g \cdot H \tag{9}$$

and the time-derivative of the energy $\dot{E}_{\text{tot}}$ describes the aircraft's real power imbalance, i.e. whether the total energy level is increasing for instance due to an excess of engine thrust for the current flight situation. The derivation of an engine model out of all the data is made by searching the model structure and parameter values that minimizes the error between the model-based computed reference power imbalance $\dot{E}_{\text{tot,ref(P)}}$ (with P being the parameters of the model) and the actual power imbalance $\dot{E}_{\text{tot}}$. Due to the high complexity of engine thrust models, a set of parameter values was determined (and later used) separately for each category. For each category, the problem can be formulated as:

$$P_{\text{opt}} = \text{argmin}_P \left(\sum_{\text{segments}} \left(\dot{E}_{\text{tot,ref(P)}} - \dot{E}_{\text{tot}} \right)^2 \right) \tag{10}$$

Later, in each category the vector of optimal parameter values P_{opt} is used and the corresponding power imbalance ($\dot{E}_{\text{tot,ref(P}_{\text{opt}})}$) will be compared to the actual power im-

balance $\dot{E}_{\text{tot}}$.

In practice, before being able to find P_{opt} by solving the problem of Eq. (10) the data need to be preprocessed. This preprocessing includes the detection and cleanup of erroneous data (which can for instance happen at times when some of the onboard computers are being reset) as well as bringing the individual channels to the same constant sampling rate and time base. Then, the data are searched for steady engine and quasi-steady flight conditions for which several engine and flight parameters only slightly vary inside predefined boundaries. According to these conditions the flight data are segmented resulting in time slices of steady conditions with an individual length between 60 s and 120 s. For each time slice mean values of altitude, speed/Mach number, temperature, gross weight, engine fan speed, fuel flow, and energy change are calculated and used for further evaluation. Using only mean values over data segments with steady flight conditions allows to reduce the data significantly although all necessary information is still available. An example of such segments is given in the time histories of several aircraft observation variables in Fig. 5. In the case shown in this figure, segments during cruise flight right after the aircraft climbed to 24,000 ft (7,315 m) are selected. With stabilized engine conditions the aircraft speed only contains small variations and the quasi steady flight assumption is valid.

With this method 202,797 segments were extracted from the B 737-700 data set and 5,161,814 segments from the B 737-800 data set. The estimation of the local engine influence on the recorded aircraft flight performance is performed using a regression technique on a subset of the data. These subsets are called "categories" in the following and were obtained by subdividing the five-dimensional domain (V,H,T_{stat},N_1,m_{AC}). It is possible to reliably estimate the engine model parameter values within a category only if this category contains enough segments. In the B 737-700 data set the 340 categories with the highest number of segments were selected and similarly in the B 737-800 data set the 750 categories with the highest number of segments were selected. The lowest number of segments in these categories were respectively 271 in the the B 737-700 case and 572 in the B 737-800 case. In both cases, an affine adjustment of the performance based on only three engine parameters (the fan speed N_1, the fuel flow $\dot{m}_{\text{Fuel}}$, and the Mach number

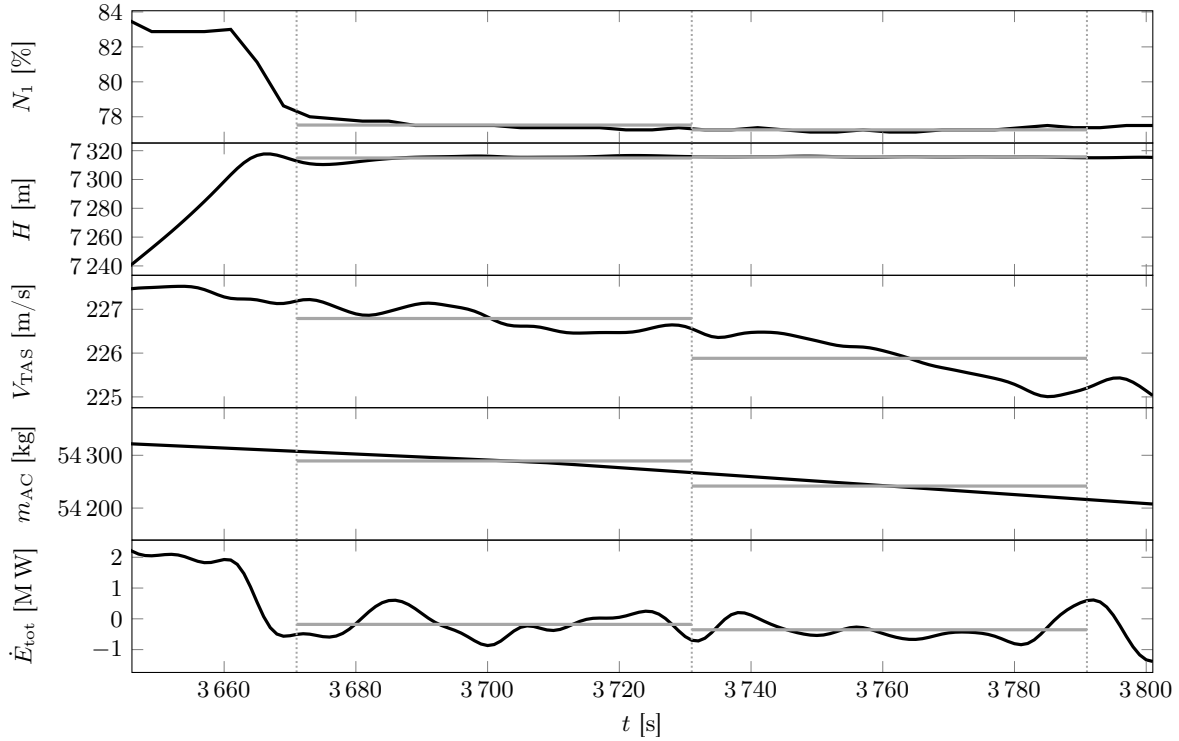

Figure 5. Example of automatically selected quasi steady segments in flight data; gray horizontal lines indicate the segments' individual mean values considered for the subsequent data analysis

Ma) was found sufficient. Note that when an affine adjustment with only 3 linear terms (one per parameter) on data sets containing several hundreds of data points is applied, there is no real risk of overfit.

Eventually, $\dot{E}_{\mathrm{tot,ref(P_{opt})}}$ (the reference power imbalance corrected from some of the unknowns affecting the engine thrust) can be written as

$$\dot{E}_{\mathrm{tot,ref(P_{opt})}} = \dot{E}_{\mathrm{tot,ref}} + \Delta f\left(N_1, \dot{m}_{\mathrm{Fuel}}, Ma\right) \ , \tag{11}$$

with $\dot{E}_{\mathrm{tot,ref}}$ being the nominal reference power imbalance and Δf being the optimal affine adjustment of the engine thrust model on the considered category.

The remaining deviations between the expected power imbalance $\dot{E}_{\mathrm{tot,ref(P_{opt})}}$ and the actual power imbalance $\dot{E}_{\mathrm{tot}}$ (rate of change of the aircraft total energy) are the variations of the flight performance within the considered aircraft fleet. These variations are known to exist and need to be characterized in order to check the feasibility of a reliable icing detection system based on the monitoring of the aircraft performance. "Reliable" includes here (among others) the need to effectively detect the performance degradation due to icing while preventing false alarms.

While the chosen energy-based approach encompasses all aspects of the flight performance and especially the couplings between the involved physical parameters, the scaling of the power imbalance $\dot{E}_{\mathrm{tot,ref(P_{opt})}} - \dot{E}_{\mathrm{tot}}$ into a nondimensional equivalent drag coefficient variation $\Delta C_{\widetilde{D}}$ eases the physical interpretation (same order of magnitude for different speeds, current lift, or even aircraft type) and later on the definition of threshold values for the detection system (see section IV). This scaling is realized as follows:

$$\Delta C_{\widetilde{D}} = \frac{\dot{E}_{\mathrm{tot,ref(P_{opt})}} - \dot{E}_{\mathrm{tot}}}{V_{\mathrm{TAS}} \cdot \overline{q} \cdot S_{\mathrm{Wing}}} \tag{12}$$

The equivalent drag coefficient $\Delta C_{\widetilde{D}}$ computed using Eq. (12) describes the aircraft flight performance variation inside the fleet, mostly but not only resulting from variation of the aircraft aerodynamic performance (e.g. due to dirt, damages, or ice accretion). Other possible causes for this variation are sensor errors, unaccounted wind influences (e.g. downdrafts), and variations in the actual engine performance.

In order to represent the data (millions of data points) in an intelligible way, convex hulls (in the ($\Delta C_{\widetilde{D}}$,C_L)-plane) corresponding to several quantiles of the data were computed and represented graphically in Fig. 6 for the B 737-700 (left) and B 737-800 (right). On these individual figures

- the black line represents the nominal drag polar of the aircraft,
- the dot-dashed gray lines are defined as by shifting the nominal drag polar by steps of 25 % C_{D0} and serve as grid in this figure,
- the dashed gray line represents an expected drag polar with moderate ice accretion comparable to Fig. 4,
- the gray area represents schematically the accuracy that the authors expect to be able to reach with performance monitoring system shown later in section IV,
- the areas defined by the dark dot-dashed, dotted gray and solid light gray polygon lines are the convex hulls of the selected data quantiles (99 %, 99.9 % and 100 %).

There are several sources of errors affecting this analysis: a limited knowledge on the engine power characteristics of these two aircraft types, a low resolution (sampling-time

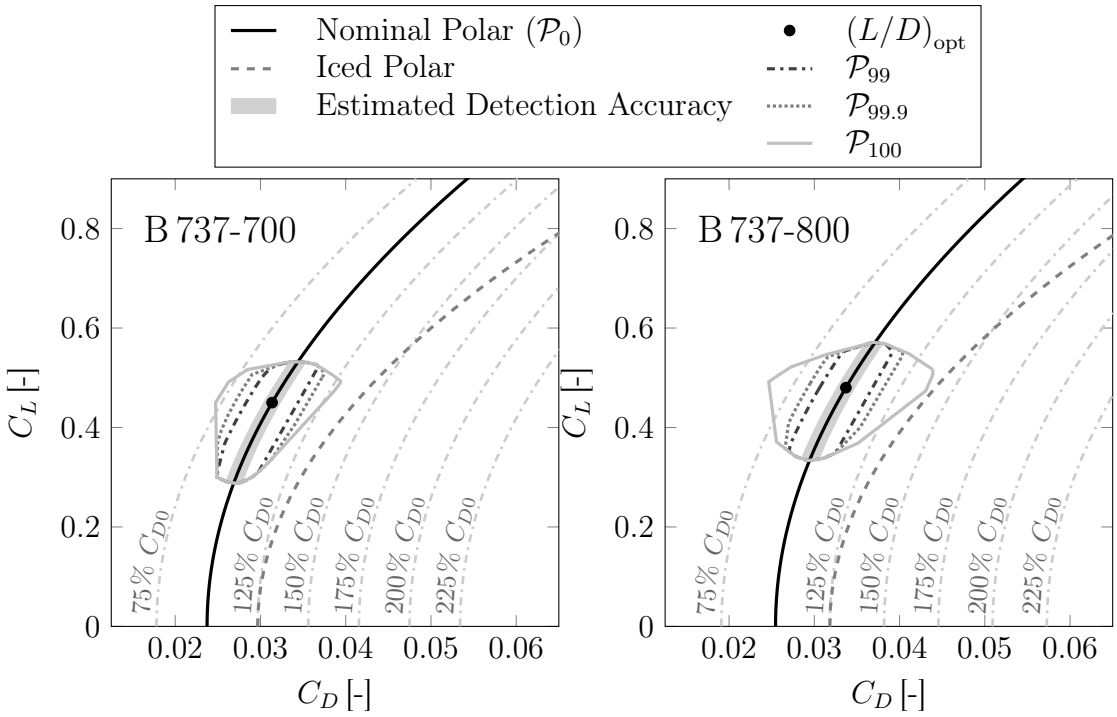

Figure 6. Obtained equivalent drag coefficient ($\mathcal{P}_{99}, \mathcal{P}_{99.9}$ & $\mathcal{P}_{100}$) within the two aircraft fleets

and quantization) of the recorded data, a missing vertical wind information (which can hardly be recovered from the data available), and the fact that the B 737-800 data include aircraft equipped with different types of winglets. Note that these sources of errors are affecting this analysis of the recorded flight data but would not affect a detection system running aboard the aircraft. After considering the knowledge gained from the data and the sensitivity of the results to the different sources of errors, an educated guess was made for the performance estimation uncertainty that can be reached in practice by an onboard system using the standard aircraft instrumentation (air data and inertial reference systems). This estimate on the achievable precision is represented by the green areas in Fig. 6.

The results of this QAR data analysis support the initial guess that it is possible to monitor the aircraft performance of all aircraft from a complete fleet using the regular sensors and with a level of precision that permits to detect the performance degradation that is induced by the ice accretion at a very early stage (before this degradation of the performance reaches a critical level). The way the QAR data was processed in the analysis presented in this section was strongly tailored to a post-flight analysis. While some of the ideas used in the various processing steps can be reused for designing a real-time onboard

detection system, numerous other refinements are needed for that application and will be shown in section IV along with the description of the detection system.

IV. Detection Methodology

In contrast to various published attempts to detect icing on changes of the dynamic aircraft behavior [12–17, 38], the proposed method is focused on the flight performance changes. It is commonly known, that icing mainly affects the aircraft's drag (see Fig. 4), but none of these available methods is based on this effect. A major advantage of "only" monitoring flight performance characteristics and not the aircraft's dynamic behavior is that no (additional) dynamic excitation is required. Such an excitation is not acceptable during normal operations as stated in Ref. [15] and especially not when flying with an aircraft which has a reduced maximum lift angle of attack due to icing.

In Ref. [37] a complete determination of the remaining flight envelope is attempted, but to the present paper authors' opinion it is extremely difficult to determine reliably the remaining flight envelope for all kinds of ice shapes. The behaviors observed on different ice shapes (see e.g. Ref. [28]) significantly differs from each other and in many cases no significant change of the aerodynamic derivatives will be observable as long as the aircraft is sufficiently far from its maximum angle of attack. With other words, approaching the stall angle of attack is required to be able to observe a change in the derivative: at this point the pilots have very little time left to react and moreover, as long as they have not increased the airspeed, the pilots can hardly increase the load factor without risking stalling. Whilst, the work of Ref. [37] does provide an interesting way of displaying the remaining envelope to the pilots, the authors think that a performance-based approach is more simple and will be both more reliable and provide a detection/warning earlier and even when still far from the boundaries of the remaining flight envelope, which are two highly desirable advantages for increasing the flight safety.

The basic idea of the herein proposed detection method is to compare the current (possibly ice-influenced) aircraft flight

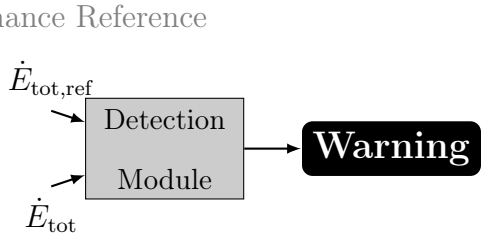

performance characteristics with a known reference, as schematically represented in Fig. 7. The energy-based flight performance analysis performed in the section is quite similar to the approach shown in section III, but the requirements and the data are very different (real-time detection vs. offline analysis, need for coping with dynamic motion vs. steady state, etc.). As a consequence the computation differs significantly. The flight performance can be formulated as a power imbalance (change of total energy) $\dot{E}_{\text{tot}}$ in both cases (current state and reference), which allows to represent the changed aircraft characteristics in only one significant value and reduces the detection module complexity. Moreover, it combines the influences of aerodynamics and engines on the aircraft performance. The power imbalance $\dot{E}_{\text{tot}}$ is analytically derived through:

$$\dot{E}_{\text{tot}} = \quad V_{\text{TAS}} \cdot \dot{V}_{\text{TAS}} \cdot m_{\text{AC}} + \frac{1}{2} \cdot V_{\text{TAS}}^2 \cdot \dot{m}_{\text{AC}} + g \cdot \dot{H} \cdot m_{\text{AC}} + g \cdot H \cdot \dot{m}_{\text{AC}} \ , \tag{13}$$

with the altitude change $\dot{H}$ referenced to the surrounding air. The same scaling/conversion of this power imbalance into an equivalent drag coefficient variation as for the analysis of section III is used:

$$\Delta C_{\widetilde{D}} \approx \frac{\dot{E}_{\text{tot,ref}} - \dot{E}_{\text{tot}}}{V_{\text{TAS}} \cdot \overline{q} \cdot S_{\text{Wing}}} \tag{14}$$

This nondimensional value is now well comparable to a predefined threshold and indicates an abnormal performance variation when exceeding the threshold value, independent from any flight point.

The fleet data evaluation in section III provides some concrete and objective data to define a suitable detection threshold, which guarantees a minimum expectable false detection rate with the standard sensors and all possible influences on flight performance during normal airline operation. Based on the results shown in Fig. 6 a threshold value of

$$\left(\Delta C_D\right)_{\text{crit}} = 30\,\%\ C_{D0} \tag{15}$$

seems adequate: it suitably exceeds the detected performance variation. Generally speaking the choice of such a threshold is always trade-off between sensitivity and the probability of generating false alarms. For a given threshold value, the risk of generating false alarms might be reduced by improving the processing or by activating the system only under some particular conditions (e.g. for icing this could be based on some range of outside air temperature). The need to prevent false alarms as much as possible results from the fact that they could induce hazardous reactions (e.g. from the pilots) in otherwise totally safe situations. Even though this is not part of the scope of the present paper, it should be noticed that the risk of inducing hazardous reactions can be alleviated by a good human-machine interface design (making messages very understandable and precise to prevent confusion and misinterpretation) and by defining good procedures (i.e. basically directly providing the description of the right reaction). In combination with a good human-machine interface and good operating procedure, a lower threshold than in Eq. (15) is probably desirable e.g. for earlier detection.

IV.A. Reference Model for the Aircraft Performance

The reference for the flight performance can be formulated in different ways, but in any case it must allow the computation of the aircraft energy evolution $\dot{E}_{\mathrm{tot,ref}}$ (power imbalance) for all relevant flight conditions. This power imbalance depends mainly on the atmospheric conditions, the aerodynamic properties of the aircraft, and the engine thrust. The aerodynamic properties of the (nominal) aircraft are usually very well known for the clean configuration, but a precise representation of the aerodynamic performance with spoiler/speedbrake deflections, high-lift, and/or gear extension might be more demanding. Furthermore, the changes through a different aircraft longitudinal trim (e.g. due to center of gravity position) should ideally also be considered in the reference. The system designer might choose to neglect some of the effects and as it will be seen later, there are easy ways to prevent that the detection system misbehave in the neglected situations.

One possible implementation of the reference model would be to use a multi-dimensional table with values of $\dot{E}_{\mathrm{tot,ref}}$, which can be interpolated to obtain intermediate values between grid points. Each dimension represents one parameter describing the aircraft,

atmosphere, or engine state. In principle, the flight performance related energy change depends on altitude, airspeed, fan speed, and lift as well as an aircraft configuration. For each of these dimensions, there is usually several measurable parameters containing comparable information. For example altitude, static pressure and air density (among others) provide a relatively similar information to the performance reference model and the table could be built based on any of these variables. Similarly, several parameters could be used for airspeed (e.g. $V_{\mathrm{TAS}}, V_{\mathrm{IAS}}, V_{\mathrm{CAS}}, Ma$, etc.), engine state (e.g. engine pressure ratio, exhaust gas temperature, etc.), or lift force.

Note that the lift force is not always equal to the weight and the aerodynamic performance must be based on the lift force in order to be applicable in all conditions and especially during turns. The model quality of the tabular model depends on the used grid size, because smaller steps between the grid points allow to better cover nonlinearities in the characteristics. The table can be generated using various sources of information: model trim calculation of a dynamic aircraft model, flight data of corresponding flight conditions, etc. and must only be created once for a given combination of aircraft and engines. The reference model used hereafter is based on the previously described table structure, but any other type of implementation could be used in principle.

IV.B. Challenges for Reliable Onboard Flight Performance Estimation

During flight, current performance state $\dot{E}_{\mathrm{tot}}$ results from Eq. (13) using measurements of true airspeed V_{TAS} and altitude H as well as an information about the current aircraft gross weight m_{AC}. The mass change $\dot{m}_{\mathrm{AC}}$ of an civil aircraft is assumed to be directly correlated to the fuel flow $\dot{m}_{\mathrm{Fuel}}$ in all engines. The altitude time derivative $\dot{H}$ corresponds to the aircraft climb respectively sink rate and is normally also available in good quality from different sensors in flight.

The airspeed V_{TAS} is derived from several measurements and contains a combination of aircraft flight path velocity and wind speed (both to be understood as 3D vectors). Its derivative, $\dot{V}_{\mathrm{TAS}}$, consequently also contains a component related to the change of both the altitude and inertial velocity vector as well as a component related to the change of wind vector. Only the first of these two components is relevant for the aircraft performance and

the second component should be ignored/removed in order to prevent it from falsifying the performance estimate.

The true airspeed time derivative can be separated in two parts

$$\dot{V}_{\mathrm{TAS}} = \dot{V}_{\mathrm{TAS},\dot{\vec{V}}_{\mathrm{k}}} + \dot{V}_{\mathrm{TAS},\dot{\vec{V}}_{\mathrm{w}}}, \tag{16}$$

where $\dot{V}_{\mathrm{TAS},\dot{\vec{V}}_{\mathrm{k}}}$ is the airspeed change due to the inertial acceleration of the aircraft and $\dot{V}_{\mathrm{TAS},\dot{\vec{V}}_{\mathrm{w}}}$ denotes the airspeed variation due to the encountered wind. The encountered wind can be estimated reliably for example by applying proper filter algorithms on measured air and ground speeds.

A variable wind corrected energy change $\dot{E}_{\mathrm{tot,corr}}$ results from Eq. (13) by using $\dot{V}_{\mathrm{TAS},\dot{\vec{V}}_{\mathrm{k}}}$ as an airspeed change:

$$\dot{E}_{\mathrm{tot,corr}} = V_{\mathrm{TAS}} \cdot \dot{V}_{\mathrm{TAS},\dot{\vec{V}}_{\mathrm{k}}} \cdot m_{\mathrm{AC}} + \frac{1}{2} \cdot V_{\mathrm{TAS}}^2 \cdot \dot{m}_{\mathrm{AC}} + g \cdot \dot{H} \cdot m_{\mathrm{AC}} + g \cdot H \cdot \dot{m}_{\mathrm{AC}} \tag{17}$$

In Eq. (17) the acceleration due to the gravity is assumed constant. A mathematically equivalent way to correct the energy change for variable wind influences is to subtract the wind change influence from the energy change $\dot{E}_{\mathrm{tot}}$ calculated with Eq. (13):

$$\dot{E}_{\mathrm{tot,corr}} = \dot{E}_{\mathrm{tot}} - V_{\mathrm{TAS}} \cdot \dot{V}_{\mathrm{TAS},\dot{\vec{V}}_{\mathrm{w}}} \cdot m_{\mathrm{AC}} \ . \tag{18}$$

With the above correction, the energy change and the corresponding equivalent drag coefficient variation in a symmetric flight condition are available and can be used for abnormal flight performance detection. To further apply the methodology to asymmetric flight conditions, the additional drag due to an angle of sideslip β must be compensated since it is detected because the performance model used (see section IV.A) does not include this effect. This can be made by inserting a compensation term $\Delta C_{D\beta,\mathrm{comp}}$ in the equation of the estimated equivalent drag coefficient variation introduced in Eq. (14) as follows:

$$\Delta C_{\widetilde{D}}(\beta) = \frac{\dot{E}_{\mathrm{tot,ref}} - \dot{E}_{\mathrm{tot,corr}}}{V_{\mathrm{TAS}} \cdot \overline{q} \cdot S_{\mathrm{Wing}}} - \Delta C_{D\beta,\mathrm{comp}} \tag{19}$$

The compensation term $\Delta C_{D\beta,\mathrm{comp}}$ can be computed based on the lateral acceleration n_{y}

and the sideslip angle β

$$\Delta C_{D\beta,\text{comp}} = -\frac{n_\text{y} \cdot m_\text{AC} \cdot g \cdot \sin\beta}{\overline{q} \cdot S_\text{Wing}}, \tag{20}$$

where β could be directly measured if the aircraft is equipped with the appropriate sensors or estimated otherwise.

With the presence of ice contamination on the wing surface, the aircraft lift characteristics are altered. The shape of the ice accretion directly impacts the change in the aircraft's lift curve. With a significant deviation from the basic aircraft's lift curve a different angle of attack is necessary to obtain a similar lift from the wing for any given airspeed. In that case, the reference model as proposed in section IV.A would give a wrong energy change for the current lift condition, assuming a lower angle of attack, and the additional drag could be underestimated. In order to cancel this effect, an additional compensation term is proposed

$$\Delta C_{D\alpha,\text{comp}} = (n_\text{z} \cdot \sin\alpha + n_\text{x} \cdot \cos\alpha) \cdot \frac{m_\text{AC} \cdot g \cdot \sin\Delta\alpha}{\overline{q} \cdot S_\text{Wing}} \tag{21}$$

using the angle of attack difference $\Delta\alpha = \alpha - \alpha_{ref}$. The reference α_{ref} corresponds to the nominal angle of attack for this airspeed and lift/load factor, which can be computed based on the nominal aerodynamic model and/or stored in an additional multi-dimensional reference table. Note that this compensation significantly increases the complexity of the detection system and roughly doubles the resources needed (CPU, memory) while only compensating a relatively small error, as it can be observed on the results of section V.A.

Rapid changes of wind (e.g. due to gust or turbulence) are too fast to be really relevant for the performance estimation: the best way to deal with them is certainly to apply a low-pass filter on the wind estimation and/or on $\Delta C_{\widetilde{D}}$ to cut off high frequency oscillations far larger than the possible performance change rates.

IV.C. System Implementation

A more detailed overview of the proposed method is given in Fig. 8. The incoming measurements are preprocessed to estimate the geodetic quasi steady wind field and suitably convert all data for the further steps. The multi-dimensional table (see section IV.A) used as reference model delivers the energy change $\dot{E}_{\mathrm{tot,ref}}$ expected for the current flight condition. The current true performance state $\dot{E}_{\mathrm{tot}}$ is for example evaluated according to Eq. (13) and corrected for wind, sideslip, and lift change inside the detection module. This module finally triggers a warning flag if the additional calculated drag coefficient $\Delta C_{\widetilde{D}}$ exceeds some predefined threshold $(\Delta C_D)_{\mathrm{crit}}$.

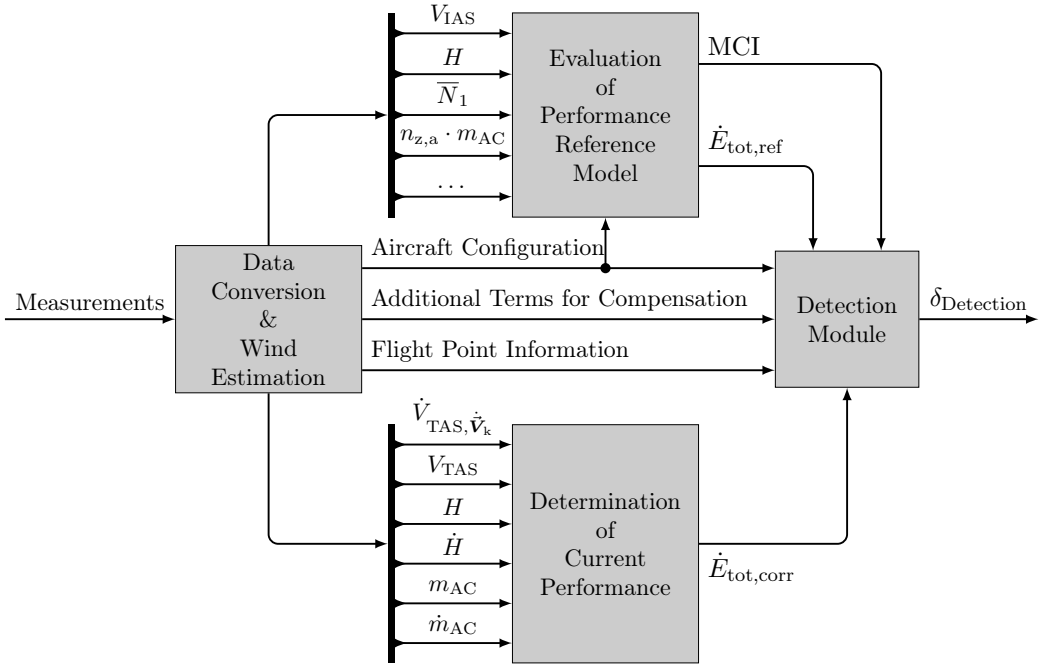

Figure 8. Possible implementation of the detection system

In the implementation presented here and used for producing the results of section V, the reference model does not account for any spoiler deflections, which significantly increase the aircraft's drag and decrease its lift. Within the normal flight operations, spoilers are only deflected during short periods of time, but speedbrakes might be used during longer periods of time. Therefore it is found suitable to reduce the complexity of the reference model by not modeling asymmetrical spoiler deflections within the multi-dimensional tables. Including speedbrake drag in the model would enable the use of the detection system during the time they are extended, however it can be argued that the

pilots would only be using the speedbrakes when being in a too high energy state (trying to descend and/or decelerate quickly) which are not the situations for which the proposed ice detection system is required. As a consequence, not covering speedbrake extension in the performance model can be an practicable option.

If spoiler/speedbrake deflection influences are not included in the reference model, the corresponding drag could be detected as a potentially icing-induced drag increase. This is prevented by defining and computing a confidence index (MCI) based on the reference model validity domain. In the case of spoiler/speedbrake extensions and also during aircraft configuration changes, this confidence index drops to zero in the current implementation and the detection algorithm is paused (in a frozen state) during that time. Note that this strategy is a design choice and by no means a limitation of the presented approach: the corrected handling of spoiler effects can be done by simply using a reference model of the aircraft flight performance which includes these effects.

With all the presented corrections and a proper post-processing of $\Delta C_{\widetilde{D}}$, the herein proposed detection methodology gets robust against various influences and disturbances resulting in a minimum rate of false-positive detections. This behavior is essential for pilot's trust in the warning from a detection system.

V. Results

The novel energy-based icing detection method introduced in section IV is applied to the DLR A 320 "ATRA" simulation model and tested hereafter with various scenarios. This model is a complete nonlinear flight dynamics model, including models for the sensor systems as well as advanced control laws and autopilot functions. This model has been extended to include a generic icing case as previously illustrated in Fig. 4. The icing severity parameter k_{ice} (similar to the definition in Ref. [12]) allows a continuous transition from the clean case (no ice $\Leftrightarrow$ $k_{\text{ice}} = 0$) to the case shown in Fig. 4 ($k_{\text{ice}} = 1$).

V.A. Icing Encounter

The purpose of the ice detection system is to detect early and reliably the performance degradation induced by the ice accretion. In order to illustrate the behavior of the system, the following simulation was performed: first, a slow ice accretion is simulated with k_{ice} going linearly from 0 to 1 in 500 s. Then the iced state is kept for 140 s and finally the initial state (no ice) is restored by going to $k_{\text{ice}} = 0$ also in 500 s. This simulation was started with a trimmed horizontal flight at 11,000 ft and with an indicated airspeed of 220 kt: this corresponds to a representative holding condition in the neighborhood of an airport. The autopilot and autothrust hold this altitude and speed constant in spite of the disturbances caused by the ice accretion. Figure 9 shows the behavior of the main parameters. The icing severity parameter k_{ice} follows the aforementioned time evolution. The real power imbalance $\dot{E}_{\text{tot,corr}}$ is always almost 0 since the aircraft continues its flight at constant speed and altitude, but the increased thrust level required for that leads the reference model to predict a significant power imbalance (large positive $\dot{E}_{\text{tot,ref}}$). The difference between $\dot{E}_{\text{tot,ref}}$ and $\dot{E}_{\text{tot,corr}}$ leads in turn to a significant increase of the equivalent drag increase $\Delta C_{\widetilde{D}}$. By comparing $\Delta C_{\widetilde{D}}$ with the real drag increase C_D, it appears that they match pretty well. The drag increase is slightly underestimated, due to the phenomena describe earlier and that could have been compensated by using the formula of Eq. (21) but this compensation term was not used here in order to illustrate that this term might be neglected.

Apart from this slight underestimation of the drag increase, a small phase-shift can be observed between C_D and $\Delta C_{\widetilde{D}}$: this results from a low-pass filter used on $\Delta C_{\widetilde{D}}$ to prevent false detection when sudden variations occurs, e.g. due to some gust or some non-physical effects (reset of an onboard computer during flight, entry of a corrected mass in the flight management system when possible). An additional safety against spurious changes of the detection flag/alarm can also be seen here: the status of the flag $\delta_{\text{Detection}}$ only changes if the difference between $\Delta C_{\widetilde{D}}$ and $(\Delta C_D)_{\text{crit}}$ has kept the same sign for a predefined time. Also a parameter that needs to be tuned based on the trade-off between sensitivity/reactivity of the system and false alarm rate.

Due to the reduced lift slope with ice present on the aircraft lifting surfaces, the current

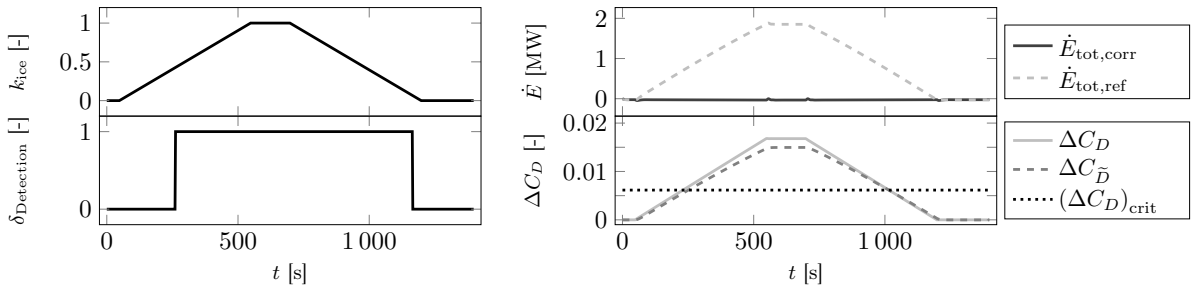

Figure 9. Behavior of the detection system during slow aerodynamic changes of the A 320 due to icing

drag is underestimated in Fig. 9 as mentioned in section IV.B. The difference between the current angle of attack α and the reference value α_{ref} can be used to evaluate the correction term $\Delta C_{D\alpha,\text{comp}}$ given in Eq. (21), which allows to properly match the true drag coefficient ΔC_D with the predicted and corrected value $\Delta C_{\widetilde{D}} + \Delta C_{D\alpha,\text{comp}}$. Figure 10 visualizes these different angle of attacks and the corresponding correction for the investigated case in the simulation.

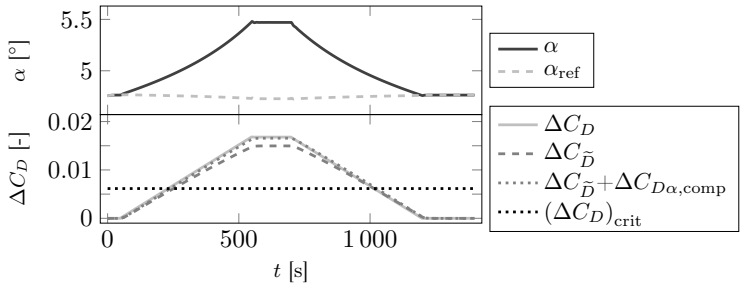

Figure 10. Behavior of the predicted drag change during slow aerodynamic changes of the A 320 due to icing including an angle of attack correction

V.B. Behavior in the Presence of Turbulence and Wind Shear

As it has been recognized in the derivation of the flight performance equations and explained in section IV.B, the temporal variation of the encountered wind poses some challenges for the design of a robust and reliable ice detection system on the basis of the aircraft performance. A scenario showing the behavior of the detection system when encountering wind changes in different frequency bands is shown in Fig. 11. The signals shown on the right side in this figures are defined exactly as in Fig. 9. On the left side, the simulated and estimated wind components (North-East-Down) are shown. The Kalman filter used for estimating the wind removes the high-frequency variations of the wind (which are not directly relevant for the flight performance) but tracks otherwise

quite well the low and medium frequency changes of the wind vector. The encountered wind shear (change in wind velocity and orientation) is quite strong and the autopilot eventually rejects the corresponding change of energy but a significant transient response ($\dot{E}_{\mathrm{tot,corr}}$ and $\dot{E}_{\mathrm{tot,ref}}$ deviations from 0) occurred. However, the equivalent drag coefficient remains almost at zero during the whole simulation, which corresponds exactly to the desired behavior.

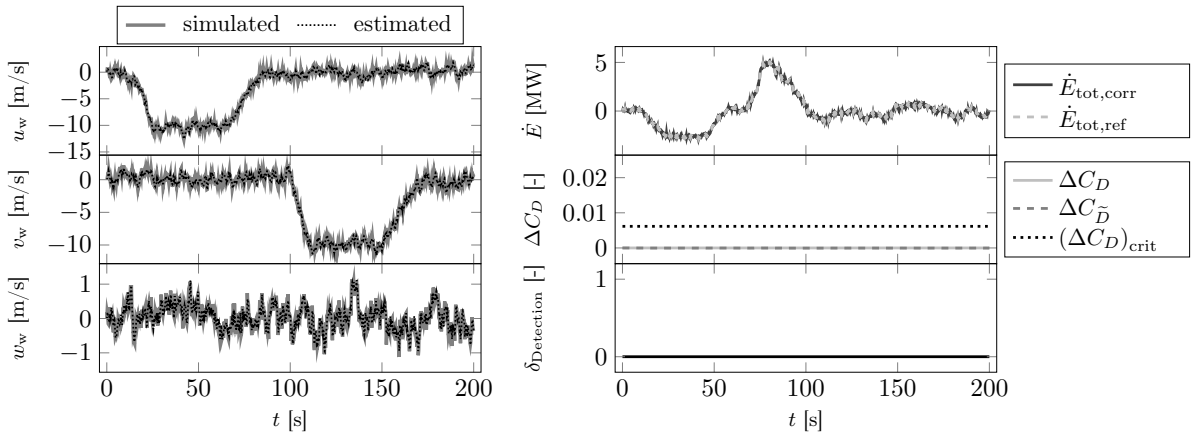

Figure 11. Behavior of the detection system in the presence of turbulence and wind shear

V.C. Behavior during Microburst Encounter

Aside from wind shear, which is above modeled as a horizontal wind change, a microburst [39] also contains a significant vertical wind component, which is illustrated in Fig. 12. The wind estimation and compensation presented in section IV.B allows to account for the strong downwind during a microburst encounter, which could prevent false alarms. In Fig. 13, time histories of wind velocity components (North-East-Down) for the simulation of such an encounter are presented, similar to the illustration of wind shear in Fig. 11. During the downwind encounter, which is starting at 20 s of simulation time, the energy level is reduced and the autopilot tries to compensate the deviation from the desired flight path with suitable control inputs and a thrust increase, which causes the energy

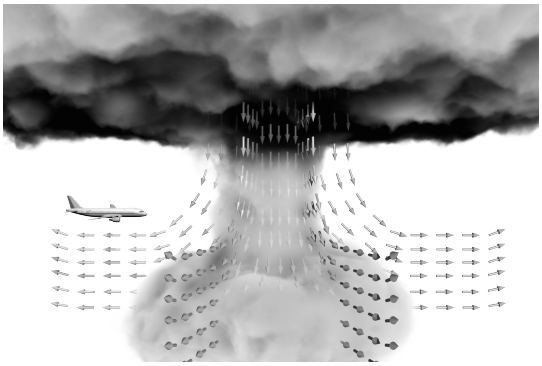

Figure 12. Illustration of microburst encounter

level to rise again. Because of the wind estimation and corresponding compensation, the measured energy change $\dot{E}_{\text{tot,corr}}$ follows the expected values of $\dot{E}_{\text{tot,ref}}$ and no false drag coefficient change or detection is observed.

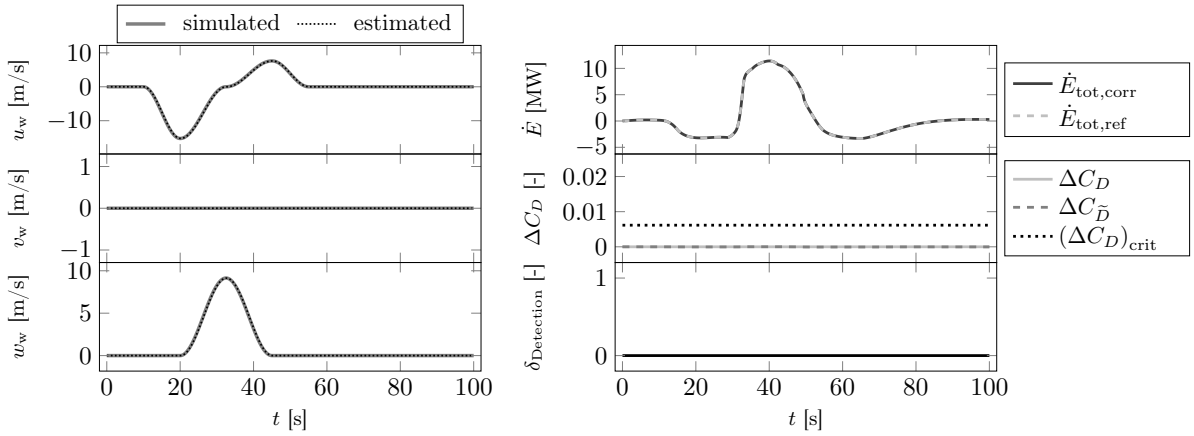

Figure 13. Behavior of the detection system during microburst encounter

V.D. Precision of the Sideslip Compensation

When using a reference performance model that only includes the performance during symmetrical flight (no sideslip), the additional drag that would be caused while slipping could be detected as an ice-induced performance degradation. This is prevented using the compensation term introduced in Eqs. (19) - (20). In order to illustrate that a purely longitudinal performance model can indeed be precisely corrected by these terms to correctly handle sideslip conditions, a steady heading sideslip (with $\beta = 10°$) scenario was simulated (see Fig. 14). A sideslip of 10° is quite extreme, but constitute a meaningful test case and permits here to show that the proposed sideslip compensation is not restricted to very small sideslip angles. The sideslip compensation term is almost perfectly equal to the detected additional drag coefficient, such that the equivalent drag coefficient is almost zero.

V.E. Control Inputs

This last scenario in Fig. 15 illustrates the behavior of the developed system during active maneuvers on all three axes: pitch, roll, and yaw. During the pitching maneuver $\dot{E}_{\text{tot,corr}}$ and $\dot{E}_{\text{tot,ref}}$ match very well. This results from the consideration of load factors

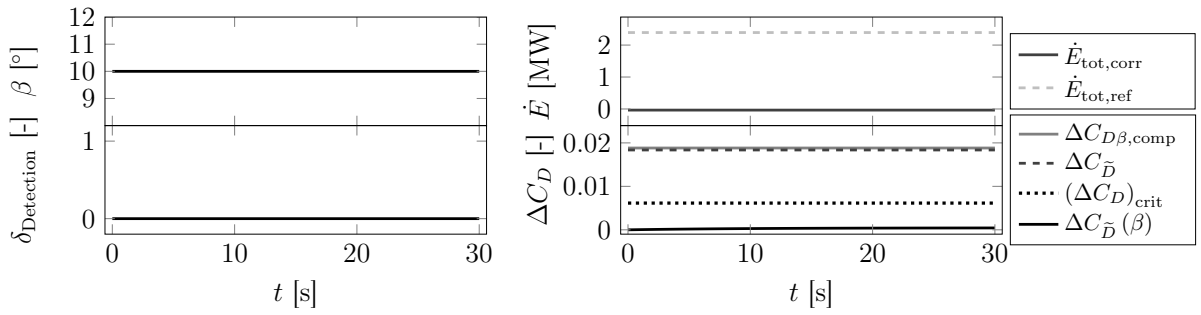

Figure 14. Behavior of the detection system during steady heading sideslip with $\beta = 10°$

different than one in the reference model. The dynamical sideslip lead to three very significant nadirs in the $\dot{E}_{\text{tot,corr}}$ curve: as expected the aircraft is losing energy (too much drag compared to the thrust) whereas the reference model does not predict it correctly since it contains no sideslip dependency. However, here again the sideslip drag coefficient compensation term follows the equivalent drag coefficient variation very well and prevents any false detection. During the final roll maneuver, which results in a large bank angle variation, the calculated and predicted energy changes are matching again.

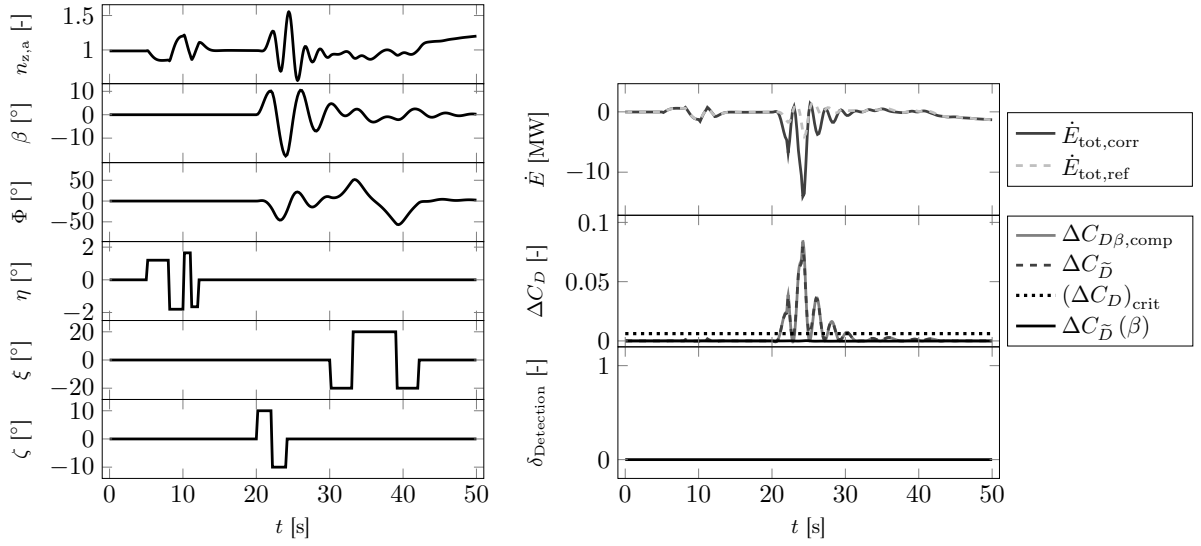

Figure 15. Behavior of the detection system during dynamic maneuvers (aircraft in "direct law")

V.F. Sensor Error Influence

Apart from external influences due to atmospheric disturbances and maneuvers, the behavior of the novel icing detection methodology in the presence of imperfect sensor readings is investigated. The method is based on the energy change with respect to the surrounding atmosphere. Consequently, the inflow and pressure altitude measurements are assumed to be critical for the reliability of the detection.

Based on the typical order of magnitude of each physical parameter involved in Eq. (13), the orders of magnitude of the four terms of Eq. (13) can be determined and are given in table 2. These orders of magnitudes are converted into the corresponding equivalent drag coefficient $\Delta C_{\widetilde{D}}$ based on the assumed order of magnitude $\mathcal{O}\left(V_{\mathrm{TAS}}\overline{q}S_{\mathrm{Wing}}\right) = 10^9$ for the denominator in Eq. (14). The first part of Eq. (13) containing the speed change $\dot{V}_{\mathrm{TAS}}$ provides the major influence on power imbalance and additional drag coefficient, followed by the third part including the altitude change $\dot{H}$. This is not surprising, because the rate of change of the aircraft mass is too small to really influence the instantaneous flight performance on typical airliners and general aviation aircraft. Consequently, the inflow and pressure altitude measurements also emerge here as main influences.

Table 2. Order of magnitude of the different parts in the power imbalance and additional drag coefficient calculation

1. part:	$\mathcal{O}\left(\dot{V}_{\mathrm{TAS}}V_{\mathrm{TAS}}m_{\mathrm{AC}}\right) = 10^6$	$\rightarrow \mathcal{O}\left(\Delta C_{\widetilde{D}}\right) = 10^{-3}$
2. part:	$\mathcal{O}\left(\frac{1}{2}V_{\mathrm{TAS}}^2\dot{m}_{\mathrm{AC}}\right) = 10^3$	$\rightarrow \mathcal{O}\left(\Delta C_{\widetilde{D}}\right) = 10^{-6}$
3. part:	$\mathcal{O}\left(g\dot{H}m_{\mathrm{AC}}\right) = 10^5$	$\rightarrow \mathcal{O}\left(\Delta C_{\widetilde{D}}\right) = 10^{-4}$
4. part:	$\mathcal{O}\left(gH\dot{m}_{\mathrm{AC}}\right) = 10^2$	$\rightarrow \mathcal{O}\left(\Delta C_{\widetilde{D}}\right) = 10^{-7}$

V.F.1. Airspeed Measurement

In modern aircraft, the air data system's airspeed measurements accuracy [40] lies within a maximum of ±5.0 kt over the entire speed range. To evaluate the detection methodology's behavior on such a measurement deviation, the airspeed sensor reading is periodically varied with $\Delta V_{\mathrm{IAS}}(t)$. A chirp signal with a variable frequency between 0.01 Hz and 5 Hz is added to the true airspeed inside the aircraft simulation model, which allows to illustrate the detection method's behavior on quasi-steady (low frequency) or dynamic sensor error. Consequently – with the airspeed indication being altered – the dynamic pressure $\overline{q}$ readings are changed in the simulation model. Figure 16 gives an impression about the simulated system behavior with the described airspeed variation. As desired, no detection is triggered due to the measured airspeed variation. Because $\dot{V}_{\mathrm{TAS},\dot{\boldsymbol{V}}_{\mathrm{k}}}$ instead of $\dot{V}_{\mathrm{TAS}}$ is used to calculate the current power imbalance, the algorithm assumes the airspeed variation to be a result of a variable wind field. Therefore $\dot{E}_{\mathrm{tot,corr}}$ is not affected

by ΔV_{IAS} in Fig. 16. But the reference model sees the variation in the measurements as a quasi-steady flight point change, which results in the mapping of the periodical airspeed reading variation in $\dot{E}_{\mathrm{tot,ref}}$. But the overall variation of the additional drag coefficient estimation $\Delta C_{\widetilde{D}}$ is far too small (e.g. at $t \approx 100\,\mathrm{s}$ in the lower right plot of $\Delta C_{\widetilde{D}}$) for leading to a false-positive warning.

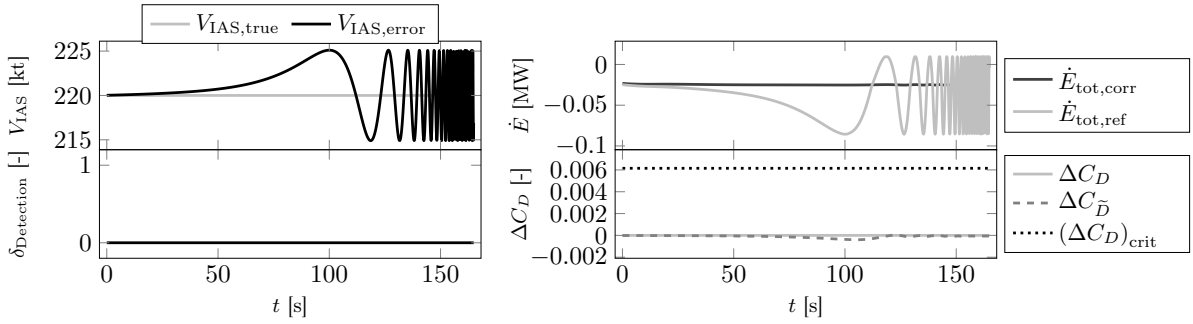

Figure 16. Behavior of the detection system with erroneous airspeed sensor readings

V.F.2. Altitude Measurement

According to the standard in Ref. [40] the maximum altitude measurement tolerance ΔH at for example 20,000 ft or below is $\pm 50\,\mathrm{ft}$. Again, a chirp signal with a variable frequency between 0.01 Hz and 5 Hz and a magnitude of 50 ft is used to simulate the quasi-steady and dynamic measurement deviation. The resulting behavior of the detection system is given in Fig. 17. Similar to the airspeed deviation in section V.F.1, the variation in the altitude measurement is interpreted by the detection algorithm as a wind field change and consequently filtered. In contrast, the simulated erroneous sensor reading manifest analog to the airspeed deviation in the determination of the power reference $\dot{E}_{\mathrm{tot,ref}}$. But the resulting error in the estimated additional drag coefficient $\Delta C_{\widetilde{D}}$ is negligible and no false detection should be expected in case of altitude measurement deviations.

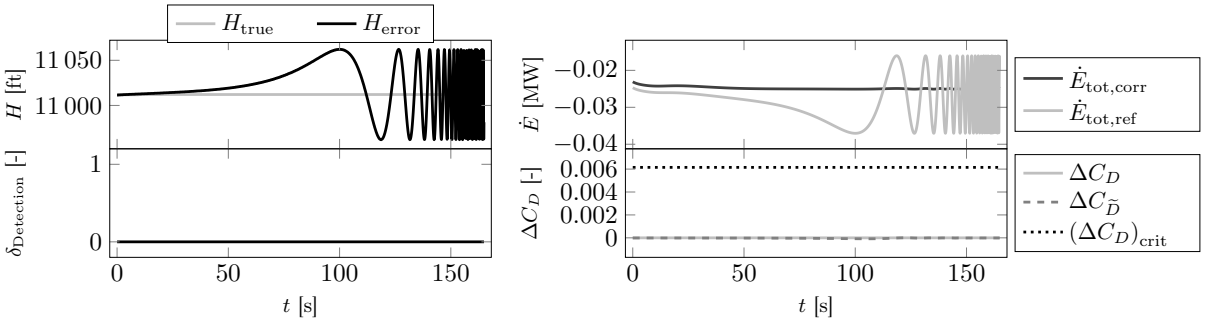

Figure 17. Behavior of the detection system with erroneous altitude sensor readings

V.F.3. Angle of Attack Measurement

Furthermore, the influence of an inaccurate angle of attack measurement is evaluated. An angle of attack error mainly affects the calculated power imbalance $\dot{E}_{\text{tot}}$ through the wind field estimation and consequently the aircraft motion calculation with respect to the surrounding air. Modern aircraft have redundant, well calibrated air data systems, which individual readings are compared against each other to prevent measurement errors. But there is still a possibility of biased measurements which could trigger false detections of icing. In the following example a maximum sensor error $\Delta\alpha$ of $\pm 0.5\,^\circ$ is used. Again, a chirp signal with the error magnitude is applied in the simulation and added to the true values. This allows also to predict the detection system's behavior on time dependent variable errors. Figure 18 shows the corresponding simulation results. In this case, the reference $\dot{E}_{\text{tot,ref}}$ is not affected, but with the variation of $\dot{E}_{\text{tot,corr}}$ an additional drag coefficient is falsely predicted for low frequency error changes. No false detection is triggered, but the example shows, that a significant angle of attack bias might result in an issue for the detection method.

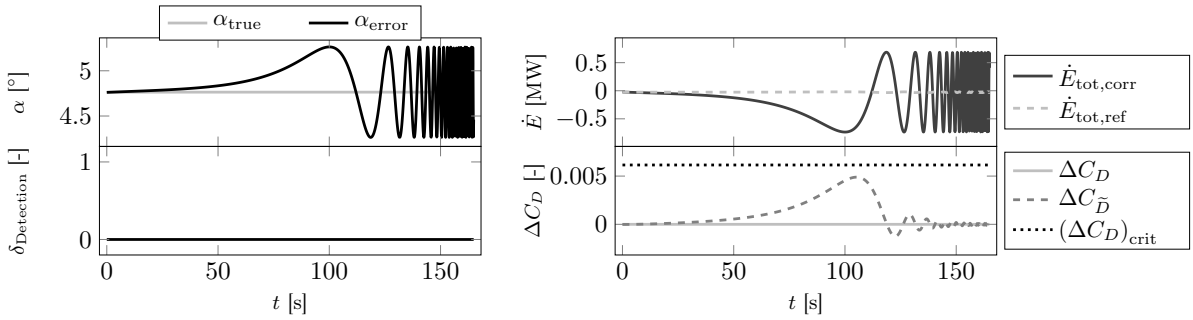

Figure 18. Behavior of the detection system with erroneous angle of attack sensor readings

V.G. Summary of the Results

For all the cases on which the system was tested in simulation (including those not shown here), the system was able to detect the performance degradations that were introduced to the aircraft but no false alarms were generated when confronted with unsteady wind or maneuvers. Moreover, the analysis of the system behavior in presence of erroneous sensor readings shows that the sensitivity of the method to the different sensor error cases tested is low. Nevertheless, proper sensor fault detection algorithm should ideally be used

in combination with the proposed system.

VI. Simulator Trials

The benefit of the ice detection in operational flight situations was evaluated during a flight simulator campaign in Spring 2016 at DLR's simulation facility AVES [41] (*AirVEhicle Simulator*, see Fig. 19(a)) in Braunschweig. The full-motion Airbus A 320 simulator provides various capabilities for testing new systems in a realistic environment. The corresponding aircraft simulation model was developed and identified by DLR using flight test data recorded with the research aircraft "ATRA". The detection method was implemented in the AVES simulator framework and integrated in the A 320 system architecture. An additional *Master Caution* chart for the flight warning computer allows to display a message on the upper ECAM display in the cockpit (see Fig. 19(b)) to inform the pilots about the detected degradation in case of a transition of $\delta_{\text{Detection}}$ from 0 to 1.

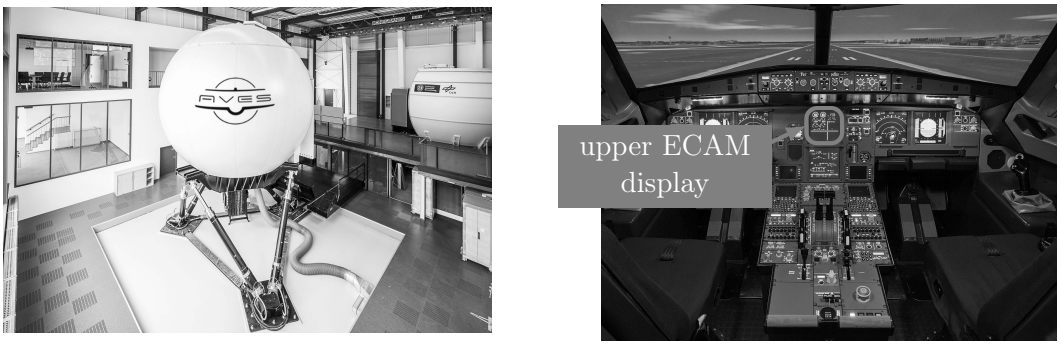

(a) simulator facility (b) A 320 cockpit in the AVES

Figure 19. DLR's AirVehicle Simulator (AVES) in Braunschweig

The experiment's main objective was to show the detection methods capability to warn pilots about the aircraft's performance degradation in situations, in which they are not able to extract the necessary information from the aircraft parameters displayed in a modern airliner's cockpit. A suitable scenario set up was designed to reach this goal. Because German airliner pilots were used as test candidates, the approach on Frankfurt International Airport was selected for the experiment. Within the scenario design it was assumed and confirmed through the pilot interviews that all candidates are well familiar with the airport, standard approaches and corresponding procedures. Consequently there should be no influence on the experiments results from e.g. pilots' increased workload due

to orientation issues during the approach. Moreover the simulator trial were a part of the demonstration of supporting system for low noise approaches, so the test candidates did not know about the icing test. Therefore pilots were not focused on icing, which was desired to force a pilot's system monitoring behavior similar to a normal operation case.

The experiment consists of two different scenarios, which are well comparable concerning the overall task and flight path: an approach to Frankfurt airport (ICAO code: EDDF) with a landing on one of the runways in western direction (25). The main difference between both planned scenarios that in the second scenario, the crew was instructed to go into one of the standard holding pattern for a minimum time of 10 minutes before turning into final approach and landing. During the whole simulator session the pilots were guided by air traffic control which was played by a professional controller outside the simulator.

The first scenario was used as an introduction into the experiment and familiarization of the simulator characteristics in a realistic flight scenario. Starting from a trimmed horizontal flight condition (flight level 150, 270 kt IAS), the aircraft was vectored along the desired flight plan over the way points KERAX, EBIPA, DF626 and REDGO to a final approach on runway 25C in Frankfurt (see Fig. 20).

In the second scenario, ATC informed the flight crew, that the instrument landing system on runway 25C was temporary unserviceable, and that a holding over way point KERAX was required, which is a standard procedure in Frankfurt. During this time of flight inside clouds with low visibility, rain and temperatures below freezing (indicated as shaded area around KERAX in Fig. 20) the aerodynamic characteristics of the A 320 model were degraded according to the generic icing influence defined in section II.B. After 10 to 15 minutes they were cleared to leave the holding, approach the airport via EBIPA, DF426 and NIBAP and land on runway 25R in Frankfurt. After leaving the icing area around KERAX, the aerodynamic degradation is completely removed to allow the aircraft to land without further restrictions.

For the experiment 12 test candidates, all airline or test pilots type-rated on multi-engine aircraft, were divided into two groups (6 pilots in each). The accumulated flight experience of the pilots varied between 1,600 and 15,800 hours of flight time on various

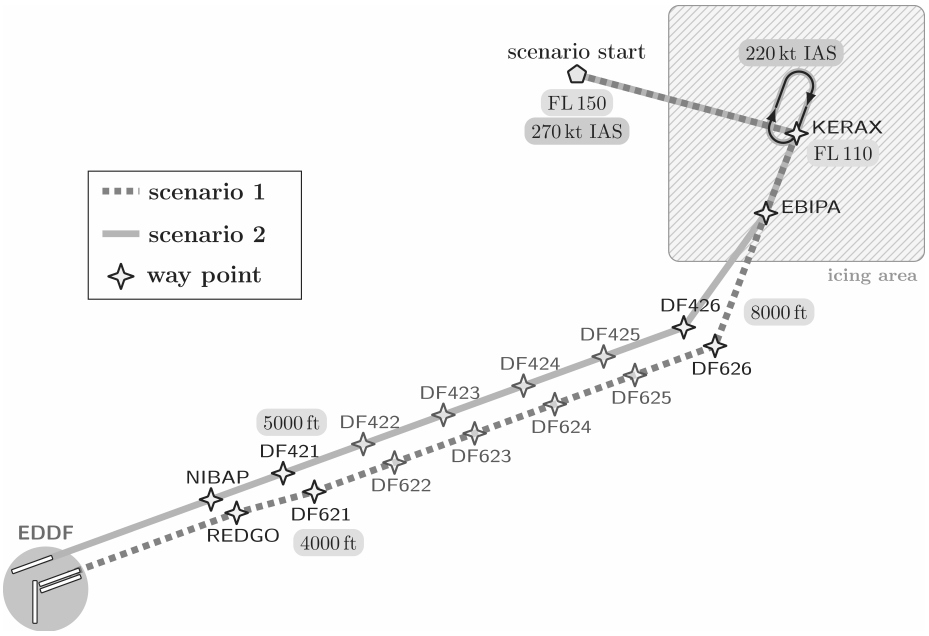

Figure 20. Flight plan for experiment scenarios – approach on Frankfurt International Airport (EDDF)

aircraft. None of the pilots was informed about the goals prior to the experiment to prevent a significant shift of their focus on the possible icing situation. But there was a briefing about the scenario flight plan in Fig. 20 for another experiment running in parallel which was focusing only the final approach. The test candidates had been briefed that the beginning of the scenario at the entry into the terminal control area was chosen to enhance their reality impression. This means that the pilots were expecting to test new assistance systems later on during the final approach and therefore they were not particularly expecting something else than regular flying to happen at the time of the icing. This corresponds to the desired pilots' mental state for the experiment. The pilots' mental state is very important for experiments strongly involving human factors and attention-related human performance. For one group of pilots the assistance system was present during the experiment and when the icing situation was automatically detected, the new type of warning message was presented to the pilots on the ECAM. This permits to define the experiment such that pilots' ability to detect the icing-related performance degradation could be compared to the enhancement gained by the displayed warning based on the new ice detection methodology. In the beginning of each simulator session, the pilots were familiarized with the (clean) A 320 aircraft model behavior, cockpit hardware, simulator motion cueing and outside view simulation during a simple takeoff and landing scenario in Frankfurt. The pilots were advised to monitor the aircraft systems

as in normal operational flight and announce any discrepancies from their expectations, even during the familiarization. It was assumed that the pilots have a certain intuition to find differences between the simulator and a real aircraft, which also come into account when testing their ability to detect the icing degradation. Actually, several pilots recognized that during the approach some of the speedbugs were not correctly displayed in the primary flight display during a very particular situation. These tiny differences did not play any major role for the experiments. However, this observation tends to reinforce the authors' confidence in the pilots' capability to detect small differences with the aircraft they are usually flying from memory.

After the familiarization both scenarios were performed without pause in between and the debriefing of both scenarios was performed at once at the end. During the second scenario pilots were at first surprised by the commanded holding pattern, but acted normally as they would do in operational flight by entering the pattern, asking for the new expected runway and doing the corresponding approach briefing. All flight crews activated the engine anti-ice, because they noticed the potential icing conditions, but only one candidate suggested to also activate the wing anti-icing system, which had no influence on the degradation for the sake of the experiment. Although all pilots were asked to monitor all flight parameters, none of the test candidates recognized the aircraft's performance and flight dynamic degradation during the holding.

All pilots were interviewed subsequent to the simulator trial. The test candidates were asked to complete a questionnaire about the experiment and the benefit of a system using the herein presented detection methodology in case of icing. For this evaluation, all pilots got the same questions without regard to the test group. The evaluation of the questionnaires initially revealed a good choice of the scenario: all pilots stated that the impression of flight was close to reality. Furthermore, the test candidates would found a similar system to the herein presented very helpful for there daily airline work. Figure 21 shows some results of this evaluation as box plots. In

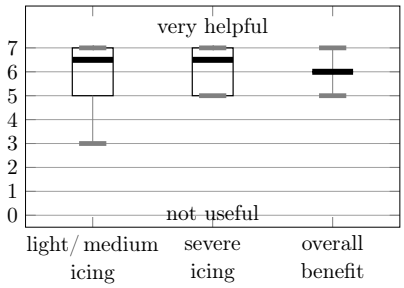

Figure 21. Pilots' opinion concerning the benefit of the ice detection system

case of light, medium and severe icing the median value of 6.5 out of 7 indicates, that the system would be helpful for the pilots to correctly interpret the current aircraft status with presence of icing. The individual results indicate that there are different opinions about the benefit in different situations: one pilot stated, that in his opinion the effects on the aircraft resulting from ice accretion in light icing condition are small enough to not being concerned about, which resulted in the low assessment of 3. But there was also one pilot arguing that especially in light icing, in which the accretion is slow and the situational awareness about the possible aircraft degradation low, the developed system would be highly beneficial. All in all, the test candidates gave a good rating of 6 for the overall benefit of the system.

VII. Conclusion

A novel ice detection method based on the monitoring of the energy state of the aircraft was presented. The validity and applicability of the approach is supported by two separated analysis. On the one hand it is supported by the analysis of the recorded data from a huge number of flights involving a fleet of aircraft from two aircraft types and during regular airline operations and on the other hand by simulations with various kinds of possible disturbances (wind, steady and dynamical maneuvers) and sensor errors. The outcome of a simulator experiment with icing in an operational flight scenario indicates that the detection system could provide the pilots a useful information about the aircraft's condition. The overall results are very promising and a patent covering all aspects of the presented system is pending.

Acknowledgement

The authors want to specially thank TUIfly, in person Friedrich Lämmle and Moritz Horejschi, for providing the herein evaluated aircraft data and their DLR colleague Dr. Fethi Abdelmoula, who converted the binary QAR flight records into MATLAB-files for easier use with DLR in house tools.

References

[1]Green, S. D., "A Study of U. S. Inflight Icing Accidents and Incidents, 1978 to 2002," No. AIAA 2006-82 in 44th AIAA Aerospace Sciences Meeting and Exhibit, American Institute of Aeronautics and Astronautics, Inc. (AIAA), Reno, Nevada, USA, January 9th - 12th 2006.

[2]N. N., *Final Report (BFU 5X011-0/98)*, Bundesstelle für Flugunfalluntersuchung, Braunschweig, DE, April 2001.

[3]N. N., *Aircraft Accident Report (NTSB/AAR-96/01, DCA95MA001), Safety Board Report*, National Transportation Safety Board (NTSB), Washington, DC, USA, July 9th 1996.

[4]N. N., "Ice Accretion Simulation," AGARD Advisory Report 344, Advisory Group for Aerospace Research & Development (AGARD) - Fluid Dynamics Panel Working Group 20, North Atlantic Treaty Organization (NATO), Neuilly-Sur-Seine, France, December 1997.

[5]Gray, V. H., "Prediction of aerodynamic penalties caused by ice formations on various airfoils," Technical Note D-2166, National Aeronautics and Space Administration (NASA), Washington, D.C., USA, February 1964.

[6]Broeren, A. P., Whalen, E. A., Busch, G. T., and Bragg, M. B., "Aerodynamic Simulation of Runback Ice Accretion," *Journal of Aircraft*, Vol. 47, No. 3, May-June 2010, pp. 924–939.

[7]Ranuado, R. J., Batterson, J. G., Reehorst, A. L., Bond, T., and O'Mara, T. M., "Determination Of Longitudinal Aerodynamic Derivatives Using Flight Data From An Icing Research Aircraft," No. AIAA 89-0754 in 27th AIAA Aerospace Science Meeting, American Institute of Aeronautics and Astronautics, Inc. (AIAA), Reno, Nevada, USA, January 9th - 12th 1989.

[8]Ratvasky, T. P. and Ranuado, R. J., "Icing Effects on Aircraft Stability and Control Determined from Flight Data. Preliminary Results," No. AIAA 93-0398 in 31st AIAA Aerospace Science Meeting and Exhibit, American Institute of Aeronautics and Astronautics, Inc. (AIAA), Reno, Nevada, USA, January 11th - 14th 1993.

[9]Lee, S., Barnhart, B. P., and Ratvasky, T. P., "Dynamic Wind-Tunnel Testing of a Sub-Scale Iced S-3B Viking," No. AIAA 2010-7986 in AIAA Atmospheric and Space Environments Conference, American Institute of Aeronautics and Astronautics, Inc. (AIAA), Toronto, Ontario Canada, August 2th - 5th 2010.

[10]Gingras, D. R., "Requirements and Modeling of In-flight Icing Effects for Flight Training," No. AIAA 2013-5075 in AIAA Modeling And Simulation Technologies (MST) Conference, American Institute of Aeronautics and Astronautics, Inc. (AIAA), Boston, Massachusetts, USA, August 19th - 22th 2013.

[11]N. N., *Federal Regulation Title 14.I.C Part 25 - Airworthiness Standards: Transport Category Airplanes*, Federal Aviation Administration (FAA), Washington, DC, USA.

[12]Bragg, M. B., Başar, T., Perkins, W. R., Selig, M. S., Voulgaris, P. G., Melody, J. W., and

Sater, N. B., "Smart icing systems for aircraft icing safety," 40th AIAA Aerospace Sciences Meeting and Exhibit, American Institute of Aeronautics and Astronautics, Inc. (AIAA), Reno, Nevada, USA, January 14th-17th 2002.

[13]Bragg, M. B., Perkins, W. R., Sarter, N. B., Başar, T., Voulgaris, P. G., Gurbacki, H. M., Melody, J. W., and McCray, S. A., "An Interdisciplinary Approach to Inflight Aircraft Icing Safety," 36th AIAA Aerospace Sciences Meeting and Exhibit, American Institute of Aeronautics and Astronautics, Inc. (AIAA), Reno, Nevada, USA, January 12th - 15th 1998.

[14]Myers, T. T., Klyde, D. H., and Magdaleno, R. E., "The Dynamic Icing Detection System (DIDS)," 38th AIAA Aerospace Science Meeting and Exhibit, American Institute of Aeronautics and Astronautics, Inc. (AIAA), Reno, Nevada, USA, January 10th - 13th 1999.

[15]Melody, J. W., Başar, T., Perkins, W. R., and Voulgaris, P. G., "Parameter Identification for Inflight Detection and Characterization of Aircraft Icing," *Control Engineering Practice*, Vol. 8, No. 9, September 2000, pp. 985–1001.

[16]Aykan, R., Hajiyev, C., and Caliskan, F., "Aircraft Icing Detection, Identification and Reconfigurable Control Based On Kalman Filtering and Neural Networks," AIAA Atmospheric Flight Mechanics Conference and Exhibit, American Institute of Aeronautics and Astronautics, Inc. (AIAA), San Francisco, California, USA, August 15th - 18th 2005.

[17]Gingras, D. R., Barnhart, B. P., Ranuado, R. J., Ratvasky, T. P., and Morelli, E. A., "Envelope Protection for In-Flight Ice Contamination," 47th Aerospace Science Meeting, American Institute of Aeronautics and Astronautics, Inc. (AIAA), Orlando, Florida, USA, January 5th - 8th 2009.

[18]Jackson, D., Owens, D., Cronin, D., and Severson, J., "Certification and integration aspects of a primary ice detection system," No. AIAA 2001-0398 in 39th AIAA Aerospace Sciences Meetings and Exhibit, American Institute of Aeronautics and Astronautics, Inc. (AIAA), Reno, Nevada, USA, January 8th - 11th 2001.

[19]Spriggs, T. J., "An ice detection system for helicopters," No. AIAA 1988-3949 in Digital Avionics Systems Conference, American Institute of Aeronautics and Astronautics, Inc. (AIAA), San Jose, California, USA, October 17th - 20th 1988.

[20]Gao, H. and Rose, J. L., "Ice Detection and Classification on an Aircraft Wing with Ultrasonic Shear Horizontal Guided Waves," *IEEE TransacTIons on UlTrasonIcs, FErroElEcTrIcs, and FrEqUEncy conTrol*, Vol. 55, No. 2, February 2009, pp. 334–344.

[21]Liu, Y., Bond, L. J., and Hu, H., "Ultrasonic-Attenuation-Based Technique for Ice Characterization Pertinent to Aircraft Icing Phenomena," *AIAA Journal*, Vol. 55, No. 5, May 2017, pp. 1602–1609.

[22]N. N., *14 CFR Parts 25 and 33 Airplane and Engine Certification Requirements in Supercooled Large Drop, Mixed Phase, and Ice Crystal Icing Conditions; Final Rule (Federal Register, Vol. 79, No. 213)*, Federal Aviation Administration, November 4th.

[23]N. N., *Certification Specifications and Acceptable Means of Compliance for Large Aeroplanes CS-25, Amendment 16*, European Aviation Safety Agency (EASA), Brüssel, Belgien, März 2016.

[24]Barnhart, B. P., Dickes, E. G., Gingras, D. R., and Ratvasky, T. P., "Simulation Model Development for Icing Effects Flight Training," General Aviation Technology Conference and Exhibition, Society of Automotive Engineers (SAE), Wichita, Kansas, USA, 16.-18. April 2002.

[25]Gingras, D. R., Dickes, E. G., Ratvasky, T. P., and Barnhart, B. P., "Modeling of In-Flight Icing Effects for Flight Training," AIAA Modeling and Simulation Technologies Conference and Exhibit, American Institute of Aeronautics and Astronautics, Inc. (AIAA), Monterey, Kalifornien, USA, 5. - 8. August 2002.

[26]Deters, R. W., Dimock, G. A., and Selig, M. S., "Icing Encounter Flight Simulator," *Journal of Aircraft*, Vol. 43, No. 5, September 2006, pp. 1528–1537.

[27]Ratvasky, T. P., Barnhart, B. P., Lee, S., and Cooper, J., "Flight Testing an Iced Business Jet for Flight Simulation Model Validation," No. AIAA-2007-0089 in 45st AIAA Aerospace Science Meeting and Exhibit, American Institute of Aeronautics and Astronautics, Inc. (AIAA), Reno, Nevada, USA, January 8th - 11th 2007.

[28]Deiler, C., "Aerodynamic Modeling, System Identification, and Analysis of Iced Aircraft Configurations," *Journal of Aircraft*, Vol. 55, No. 1, January-February 2018, pp. 145–161.

[29]Deiler, C., "Time Domain Output Error System Identification of Iced Aircraft Aerodynamics," Deutscher Luft- und Raumfahrtkongress, Deutsche Gesellschaft für Luft- und Raumfahrt (DGLR), Rostock, September 22th - 24th 2015.

[30]Jategaonkar, R., *ldentification of the Aerodynamic Model of the DLR Research Aircraft ATTAS from Flight Test Data*, Deutsche Forschungsanstalt für Luft- und Raumfahrt e. V. (DLR), Köln, September 1990.

[31]Moennich, W., "Ein 2-Punkt-Aerodynamikmodell für die Identifizierung," Symposium 'Systemidentifizierung in der Fahrzeugdynamik', Paper No 3.1 in DFVLR Mitteilung 87-22 (in German), 1987.

[32]Fischenberg, D. and Jategaonkar, R. V., "Identification of Aircraft Stall Behavior from Flight Test Data," No. 17 in RTO Systems Concepts and Integration Panel (SCI) Symposium, NATO Research and Technology Organisation, Madrid, Spain, May 5th - 7th 1998.

[33]Fischenberg, D., "Identification of an unsteady aerodynamic stall model from flight test data," No. AIAA 95-3438-CP in AIAA Atmospheric Flight Mechanics Conference, American Institute of Aeronautics and Astronautics, Inc. (AIAA), Baltimore, Maryland, USA, August 7th - 10th 1995, pp. 138–146.

[34]Deiler, C., "Time Domain Output Error System Identification of Iced Aircraft Aerodynamics," *CEAS Aeronautical Journal*, Vol. 8, No. 2, June 2017, pp. 231–244, "First Online: 04 January 2017".

[35]Bragg, M. B., Hutchison, T., Merret, J., Oltman, R., and Pokhariyal, D., "Effect of Ice Accretion on Aircraft Flight Dynamics," No. AIAA 2000-0360 in 38th AIAA Aerospace Science Meeting and Exhibit,

American Institute of Aeronautics and Astronautics, Inc. (AIAA), Reno, Nevada, USA, January 10th - 13th 2000.

[36]Krajěk, K., Nikolić, D., and Domitrović, A., "Aircraft performance monitoring from flight data," *Technical Gazette*, Vol. 22, No. 5, Oktober 2015, pp. 1337–1344.

[37]Lombaerts, T., Schuet, S., Acosta, D., Kaneshige, J., and Martin, L., "Piloted Simulator Evaluation of Maneuvering Envelope Information for Flight Crew Awareness," No. AIAA 2015-1546 in AIAA SciTech - AIAA Guidance, Navigation, and Control Conference, American Institute of Aeronautics and Astronautics, Inc. (AIAA), Kissimmee, Florida, USA, January 5th - 9th 2015.

[38]Dong, Y. and Ai, J., "Research on inflight parameter identification and icing location detection of the aircraft," *Aerospace Science and Technology*, Vol. 29, No. 1, August 2013, pp. 305 – 312.

[39]Fujita, T. T., "Downbursts and microbursts - An aviation hazard," *Preprints*, 19. Conference on Radar Meteorology, American Meteorological Society, American Meteorological Society, Miami Beach, Florida, USA, 15.-18. April 1980, pp. 94–101.

[40]N. N., *Air Data Computer - Minimum Performance Standard (Aerospace Standard AS8002)*, SAE International, Warrendale, Pennsylvania, September 1996.

[41]Duda, H., Gerlach, T., Advani, S. K., and Potter, M., "Design of the DLR AVES Research Flight Simulator," AIAA Modeling and Simulation Technologies (MST) Conference, American Institute of Aeronautics and Astronautics, Inc. (AIAA), Boston, Massachusetts, USA, 19. - 22. August 2013.